[CANCER RESEARCH 58, 3116–3131, July 15, 1998]

Expression and Location of Hsp70/Hsc-Binding Anti-Apoptotic Protein BAG-1 and Its Variants in Normal Tissues and Tumor Cell Lines[1]

Shinichi Takayama, Stanislaw Krajewski, Maryla Krajewska, Shinichi Kitada, Juan M. Zapata, Kristine Kochel, Deborah Knee, Dominic Scudiero, Gabriella Tudor, Gary J. Miller, Toshiyuki Miyashita, Masao Yamada, and John C. Reed[2]

The Burnham Institute, La Jolla, California 92037 [S. T., S. Kr., M. K., S. Ki., J. M. Z., K. K., D. K., J. C. R.]; Science Applications International Corporation Frederick, National Cancer Institute-Frederick Cancer Research & Development Center, Frederick, Maryland 21702 [D. S., G. T.]; University of Colorado Health Science Center, Department of Pathology, Denver, Colorado 80262 [G. J. M.]; and The National Children's Medical Research Center, Department of Genetics, Tokyo 154, Japan [T. M., M. Y.]

ABSTRACT

BAG-1 is a multifunctional protein that blocks apoptosis and interacts with several types of proteins, including Bcl-2 family proteins, the kinase Raf-1, certain tyrosine kinase growth factor receptors, and steroid hormone receptors, possibly by virtue of its ability to regulate the Hsp70/Hsc70 family of molecular chaperones. Two major forms of the human and mouse BAG-1 proteins were detected by immunoblotting. The longer human and mouse BAG-1 proteins (BAG-1L) appear to arise through translation initiation at noncanonical CTG codons located upstream of and in-frame with the usual ATG codon used for production of the originally described BAG-1 protein. Immunoblotting experiments using normal tissues revealed that BAG-1L is far more restricted in its expression and is present at lower levels than the more prevalent BAG-1 protein. Human but not mouse tissues also produce small amounts of an additional isoform of BAG-1 of intermediate size (BAG-1M) that probably arises through translation initiation at yet another site involving an ATG codon. All three isoforms of human BAG-1 (BAG-1, BAG-1M, and BAG-1L) retained the ability to bind Hsc70. Subcellular fractionation and immunofluorescence confocal microscopy studies indicated that BAG-1L often resides in the nucleus, consistent with the presence of a nuclear localization sequence in the NH_2-terminal unique domain of this protein. In immunohistochemical assays, BAG-1 immunoreactivity was detected in a wide variety of types of cells in normal adult tissues and was localized to either cytosol, nucleus, or both, depending on the particular type of cell. In some cases, cytosolic BAG-1 immunostaining was clearly associated with organelles resembling mitochondria, consistent with the reported interaction of BAG-1 with Bcl-2 and related proteins. Furthermore, experiments using a green fluorescence protein (GFP)-BAG-1 fusion protein demonstrated that overexpression of Bcl-2 in cultured cells can cause intracellular redistribution of GFP-BAG-1, producing a membranous pattern typical of Bcl-2 family proteins. The BAG-1 protein was found at high levels in several types of human tumor cell lines among the 67 tested, particularly leukemias, breast, prostate, and colon cancers. In contrast to normal tissues, which only rarely expressed BAG-1L, tumor cell lines commonly contained BAG-1L protein, including most prostate, breast, and leukemia cell lines, suggesting that a change in BAG-1 mRNA translation frequently accompanies malignant transformation.

INTRODUCTION

The BAG-1 protein was originally identified as a novel regulator of apoptosis by virtue of its ability to bind Bcl-2, a potent blocker of cell death (1). In gene transfer experiments using cultured cells, overexpression of BAG-1 can collaborate with Bcl-2 in suppressing apoptosis induced via CD95 (Fas/APO-1), the general kinase inhibitor staurosporine, withdrawal of survival factors from media, thymidine excess, and chemotherapeutic drugs (1–4). Overexpression of BAG-1 by itself has also been reported to inhibit or delay cell death caused by growth factor deprivation, heat shock, and p53, in at least some types of cells (1, 2, 5, 6).

Recently, BAG-1 has been reported to form complexes with several proteins, including the protein tyrosine kinase growth factor receptors for HGF[3] (scatter factor) and PDGF (7). The BAG-1 binding site in the cytosolic domain of the HGF-R appears to be required for the generation of signals by this receptor that promote cell survival. In addition, overexpression of BAG-1 has been shown to increase the metastatic potential of tumor cells *in vivo*.[4] This finding could be relevant either to the effects of BAG-1 on HGF-R, which increases cell motility (8), or to its general ability to prevent cell death, because epithelial cells undergo apoptosis when detached from extracellular matrix unless protected by anti-apoptosis proteins (9).

The expression of BAG-1 is up-regulated by some growth factors such as IL-2, IL-3, and prolactin, suggesting a role for this protein in growth factor receptor generated signals for cell survival or proliferation (2, 10). Moreover, gene transfer-mediated elevations in BAG-1 protein levels have been shown to prolong the survival of fibroblastic and hematopoietic cell lines when deprived of growth factors (1, 2) as well as neuronal cells deprived for neurotrophins (3). In an IL-3-dependent hemopoietic cell line, enforced expression of BAG-1 not only promoted cell survival but also allowed for factor-independent cell growth (2). Of potential relevance to this observation, BAG-1 can form complexes with the serine/threonine protein kinase Raf-1, causing elevations its enzymatic activity through a Ras-independent mechanism (11).

Although many details are presently lacking, the diversity of proteins with which BAG-1 interacts may be attributable to its ability to bind and modulate the activities of the 70-kDa family of molecular chaperones, including Hsp70 and Hsc70 (5). BAG-1 therefore may represent a novel component of the chaperone system that modulates interactions of Hsp70/Hsc70 with other proteins, inducing alterations in the conformations of these target proteins and thereby altering their biochemical and biological activities in cells. In this regard, BAG-1 appears to function analogous to GrpE, the bacterial ADP-ATP exchange protein that collaborates with DnaK, the bacterial equivalent of Hsp70 in prokaryotes (12). Indeed, the predicted human and murine BAG-1 proteins share 17 and 19% amino acid identity and 28 and 30% amino acid similarity with bacterial GrpE. The human and mouse

Received 8/7/97; accepted 5/18/98.

The costs of publication of this article were defrayed in part by the payment of page charges. This article must therefore be hereby marked *advertisement* in accordance with 18 U.S.C. Section 1734 solely to indicate this fact.

[1] This work was supported by Grant CA67329 from the NIH/National Cancer Institute. J. M. Z. was a recipient of a fellowship from the Fulbright/Spaniard Ministry of Education and Science and is presently supported by funds provided by the Breast Cancer Fund of the State of California through the Breast Cancer Research Program of the University of California (#3FB-0093). D. K. is a recipient of a fellowship from the Susan B. Komen Foundation, as well as a Wellcome Travel Grant.

[2] To whom requests for reprints should be addressed, at The Burnham Institute, 10901 North Torrey Pines Road, La Jolla, CA 92037. Phone: (619) 646-3140; Fax: (619) 646-3194; E-mail: jreed@burnham-inst.org.

[3] The abbreviations used are: HGF, hepatocyte growth factor; HGF-R, HGF receptor; IL, interleukin; GST, glutathione *S*-transferase; ORF, open reading frame; PDGF, platelet-derived growth factor; PDGF-R, PDGF receptor; KLH, keyhole limpet hemocyanin; PMSF, phenylmethylsulfonyl fluoride; NLS, nuclear localization sequence; bFGF, basic fibroblast growth factor; ER, estrogen receptor.

[4] A. Yawata, M. Adachi, H. Okuda, Y. Naishiro, A. Takamura, S. Takayama, J. C. Reed, and K. Imai. Prolonged cell survival enhances peritoneal dissemination of gastric cancer cells, Oncogene, in press.

BAG-1 proteins also contain a ubiquitin-like domain near their NH_2-terminal, although the functional significance of this region of BAG-1 is presently unknown (1, 13).

Recently, alternative forms of the BAG-1 protein have been reported to arise through translation initiation at different sites within the BAG-1 mRNA (14). One of these isoforms of BAG-1, which has been termed RAP46, has been shown to bind several steroid hormone receptors (15). Although the functional significance of these interactions are still being defined, the findings suggest a role of some isoforms of the BAG-1 protein in regulating nuclear proteins, in addition to cytosolic proteins.

Given the capacity of BAG-1 to promote cell survival and its penchant for augmenting the bioactivities of several proteins known to be important for tumorigenesis (*e.g.*, Bcl-2, Raf-1, HGF-R, and PDGF-R), BAG-1 can be regarded as a candidate proto-oncogene that we hypothesize may become overexpressed in certain types of tumors. To provide information about the regulation of BAG-1 protein production, therefore, we generated monoclonal antibodies against the human BAG-1 protein and used them for assessing the expression of this protein in normal human tissues and a panel of 67 human tumor lines.

MATERIALS AND METHODS

Monoclonal Antibody Preparation. Bcl-2 transgenic mice (line B6; Ref. 10) were immunized without adjuvants at 4–6 weeks of age using s.c. and i.p. injections of purified GST-BAG-1 protein encoding the last 170 amino acids of the human BAG-1 protein (500 μg of total protein). Animals were boosted four times at 1–2-week intervals with ~400 μg of GST-BAG-1 protein, and spleens were harvested 3 days after the last immunization. Splenocytes were fused with SP/02 cells, and hybridoma selections were performed in 96-well plates, as described (11). Primary screening of hybridomas was accomplished by ELISA, using GST-BAG-1 protein. Of ~1100 hybridomas screened, 51 were positive. Of these, 28 were found to react with GST-BAG-1 but not GST control protein in a secondary ELISA screen. Ten hybridomas, which reacted specifically with BAG-1 protein on immunoblots, were obtained and isotyped (eight IgG1; two IgG2b). Four of these also immunoprecipitated BAG-1 protein and were used for this study: clones KS-6C8, KS-5A6, KS-10B6, and KS-13A10. Ascites was produced in pristane-primed Balb/c mice.

Antiserum Preparation. Polyclonal antisera 1680 and 1735 were generated using a GST-mouse-BAG-1 (8-219) fusion protein (1) and a synthetic peptide NH_2-CNERYDLLVTPQQNSEPVVQD-amide representing amino-acids 26-45 of the mouse BAG-1 protein, respectively. The peptide was synthesized with an NH_2-terminal cysteine to facilitate conjugation to maleimide-activated carrier proteins KLH and OVA (Pierce, Inc.) as described previously (16). New Zealand White female rabbits were injected s.c. with either 0.25 ml of GST-BAG-1 (0.5 mg/ml) or a combination of 0.25 ml each of KLH-peptide (1 mg/ml), and OVA-peptide (1 mg/ml) mixed in an equal volume of Freund's complete adjuvant (dose divided over 10 injection sites) and then boosted three times at weekly intervals, followed by another four to eight times at monthly intervals with 0.25 mg of either GST-BAG-1 or 0.25 mg each of KLH-peptide and OVA-peptide immunogens in Freund's incomplete adjuvant before collecting blood and obtaining immune serum. The generation and characterization of a rabbit anti-mouse BAG-1 antiserum targeted against amino acids 204-219 have been described (1).

Immunoblotting. For most experiments, cells were lysed in RIPA buffer (16) containing both protease inhibitors (1 mM PMSF, 0.28 TIU/ml aprotinin, 50 μg/ml leupeptin, 1 mM benzamidine, and 0.7 μg/ml pepstatin) and phosphatase inhibitors (5 mM NaF, 2 mM sodium orthovanadate, 10 mM sodium β-glycerophosphate, 2 mM sodium pyrophosphate, 50 mM *p*-nitrophenylphosphate, and 1 μM microcystin LR). Aliquots containing 50 μg of total protein were subjected to SDS-PAGE using 12% gels, followed by electro-transfer to nitrocellulose (0.45 μm) filters. Immunodetection was accomplished using 1:1000 (v/v) dilutions of monoclonal antibody ascites or rabbit antisera, followed by appropriate secondary antibodies and ECL-based detection as described (17). For correlations with the NCI 60 tumor cell line database, data on X-ray films were quantified by scanning densitometry using the IS-1000 image analysis system (Alpha Innotech, Inc.). After collecting data for the entire panel of tumor cell lines on several immunoblot filters, residual lysates from two representative tumor lines per blot were re-analyzed together in the same blot along with a standard curve created by using GST-hu-BAG-1 protein (1–20 ng/lane). The scanning densitometry results from the GST-BAG-1 standard-containing blot were used to normalize all data before estimating the ng of BAG-1 protein per 50 μg of total protein. Data from two independent GST-BAG-1 standard-containing blots were within 20% agreement.

Immunohistochemistry. Tissues for immunohistochemical analysis were derived either from human biopsy and autopsy material or normal adult Balb/c mice. Tissues were fixed in either neutral-buffered formalin, B5, Z-Fix (Anatech, Inc.), or Bouin's solution (Sigma Chemical Co., Inc.), embedded in paraffin, and sectioned (5 μm). For experiments with rabbit polyclonal antibodies directed against the mouse BAG-1 protein, an ABC/diaminobenzidine-based detection method was used, as described in detail (18–20). Typically, the dilution of anti-mBAG-1 polyclonal antiserum used was 1:500 or 1:1000 (v/v). For immunostaining of human tissues, the ascites form of anti-huBAG-1 murine monoclonal antibodies was diluted 1:200 (v/v) and detected using a streptavidin-based enhancement method [LSAB (+) kit (Dako, Inc., Santa Barbara, CA)]. Nuclei were counterstained with either hematoxylin or methyl green.

For all mouse tissues examined, the immunostaining procedure was performed in parallel using preimmune sera. In some cases, the antisera were preadsorbed with 5–10 μg/ml of the synthetic peptide immunogen, thus providing an additional control for immunospecificity. When using the anti-human BAG-1 monoclonal antibodies, an irrelevant mouse IgG1 monoclonal (Dako) was used as a specificity control for all experiments. Occasionally, preadsorption of monoclonal antibodies with GST-BAG-1 protein was also used to assess the specificity of immunostaining. The immunostaining results were arbitrarily scored according to intensity as: 0, negative; 1^+, weak; 2^+, moderate; and 3^+, strong to very strong. Results presented for each tissue were based on consensus from immunohistochemical analysis of multiple slides.

Laser Scanning and Fluorescence Confocal Microscopy. Some of the same immunostained paraffin sections counterstained with methylgreen and used for conventional light microscopy were examined by laser scanning microscopy. For these studies, a Zeiss conventional light microscope equipped with a argon-ion laser (488-nm emission) (LSM-10) was utilized in differential interference contrast mode, essentially as described (21). Plan-apochrome ×40 dry and ×63 oil objective lenses were used. Black and white images were derived through electronic processing methods, which enhance the positive reaction signals by contrast normalization using a scaling density. Final images were printed using Adobe Photoshop software and a laser printer.

For studies involving GFP, fluorescence images were obtained using a confocal laser scanning microscope (model GB-200; Olympus, Tokyo, Japan) equipped with a triple-line Kr/Ar laser with excitation at 488 nm and detection at 500 to 530 nm bandpass.

cDNA Cloning. The human BAG-1 cDNA clones used for these studies have been described (13). The mouse BAG-1 cDNA clone SN245-9 (1) was used as a hybridization probe for screening a mouse λgt-10 kidney library, resulting in the cDNA clone SN285-13, which contains 114 bp of sequence upstream of the originally described ORF. Additional 5′ sequence data were obtained from a mouse EST clone AA15486 and from comparisons with a mouse genomic clone, which was obtained by screening a λ-FixII 129 SVJ library (Stratagene, Inc.).

Plasmid Constructions. The 1290-bp human BAG-1 cDNA pKK240 (14), which spans −390 to 880 bp relative to the AUG start codon, was subcloned into the *Eco*RI site of pcDNA3 (Invitrogen, Inc.), creating the plasmid pKK-241-1. To produce BAG-1M protein, a version of this pcDNA3-BAG-1 expression plasmid lacking most of the sequences upstream of the alternative AUG start codon at −132 bp relative to the usual BAG-1 ORF was prepared by digestion with *Sac*II and *Bam*HI, thus discarding a 256-bp fragment that was separated from the plasmid by agarose gel electrophoresis (*Sac*II is located immediately upstream of the ATG (*CCGCGG*ATGA) in the pKK240 BAG-1 cDNA; the *Bam*HI site resides within the multiple cloning site of pcDNA3). After gel purification of the residual plasmid band and blunting the ends using T4 DNA polymerase with deoxynucleotide triphosphates, the plasmid was recircularized using T4 DNA-ligase to create pSN670-2, which was transformed into XL-1 blue bacteria (Stratagene, Inc). Mutants of hu-BAG-1, in which the CTG codons at −345 and −297 were converted to ATG, were

prepared by PCR using pKK241-1 as a template and the mutagenic forward primers 5′-gggaattcAGTGCGGGC*ATG*GCTC-3′ or 5′-gggaattcGAGCGGA*TG*GGTTCCCG-3′ together with the reverse primer 5′-GCGCTCGAGCTCGGCCAGGGCAAAG-3′. After digestion of the *Eco*RI and *Xho*I sites in the forward and reverse primers, respectively, the resulting ~1.0-kbp fragments were subcloned into *Eco*RI/*Xho*I-digested pcDNA3, creating the plasmids pSN 815-2 and pSN 815-4.

For expression or *in vitro* translation of mouse BAG-1 proteins, the plasmid pRc/CMV-S33 (1), which encodes the murine 219-amino acid BAG-1 protein, was used. In addition, a longer BAG-1 cDNA (SN285-13) was subcloned into the *Eco*RI site of pSKII.

For expression of GST-huBAG-1 fusion proteins in bacteria, a partial BAG-1 cDNA (hs33-2) that had been obtained from a λgt-11 human breast library and that encodes the last 182 amino acids of the huBAG-1 protein (13) was subcloned in-frame with the GST-encoding sequences in pGEX-3X (Pharmacia, Inc.) using a PCR approach. Briefly, the hs33-2 cDNA was subcloned into the *Eco*RI site of pSK-II (Strategene, Inc.), and this plasmid was used as a template for PCR amplication with the *Bam*HI-containing forward primer 5′-GGGGATCCGTGAACCAGTTGTCCA-3′ and the reverse primer 5′-CTACACCTCACTCGGCCAGG-3′. The resulting PCR product was digested with *Bam*HI and *Bgl*II, gel-purified by gel electrophoresis in 1% Nusieve agarose, and subcloned into the *Bgl*II site of pSKII-hs33-2, which had been prepared by digestion with *Bgl*II and *Bam*HI, thus fusing the PCR product that encodes amino acids 52-171 of huBAG-1 with the distal portion of the huBAG-1 ORF encoding residues 172–230 and creating the plasmid pKK169. After confirming the correct nucleotide sequence, huBAG-1 was excised from pKK169 with *Bam*HI and *Eco*RI and subcloned into the corresponding sites in pGEX-3X, creating the plasmid pKK170. Additional GST-BAG-1 deletion mutants of pKK170 were also prepared using pKK169 and then subcloning into pGEX-3X, including: (*a*) pKK170-2, which encodes residues 132–221 of huBAG-1 (deletion of COOH-terminal 9 amino acids relative to pKK-170) by digestion of pKK169 with *Bam*HI and *Pst*I; (*b*) pKK173-1, which encodes that last 99 amino acids of huBAG-1 (132–230) by digestion of pKK169 with *Pvu*II and *Eco*RI; and (*c*) pKK-173-2, which encodes residues 52–131 (Δ COOH-terminal 99 amino acids relative to pKK170) by digestion of pKK169 with *Pvu*II and *Pst*I.

To generate a plasmid producing GFP-BAG-1, the mouse BAG-1 cDNA SN245-9 in pSKII (1) was amplified by the PCR using forward primer 5′-GGAATTCCAAGACCGAGGAGAT-3′ and reverse primer 5′-CGGGATCCAGGGCCAAGTTTGTA-3′, which have *Eco*RI and *Bam*HI linkers, respectively. The amplified product was digested with *Eco*RI and *Bam*HI, gel-purified, and subcloned into pEGFP-C1 (Clontech).

GST-Fusion Protein Production. The pKK170 plasmid encoding GST hBAG-1(52–230) was transformed into XL-1 blue *Escherichia coli* strain (Stratagene, Inc.). After overnight culture in LB with 50 μg/ml ampicillin, 2 ml of culture were transferred to 1 liter of Luria Burton-ampicillin media and grown at 37°C until the *A*600 reached ~1.0, then grown overnight at room temperature with 0.1 mM isopropyl-1-thio-β-D-galactopyranoside. Cells were then recovered by centrifugation and resuspend in 10 ml of 1× PBS (pH 7.4) containing 1% Triton X-100 and 1 mM PMSF. After freeze-thawing once, the suspension was sonicated twice on ice using a 5-mm diameter probe (Heat Systems, Inc.) at medium intensity (level 5 of 10) for 2 min. After centrifugation at ~10,000 × *g* for 20 min at 4°C, the resulting supernatant was mixed with ~2 ml of glutathione-Sepharose beads (packed volume) and rotated at 4°C for 2 h in a capped 15-ml polypropylene tube. After washing three times in the same PBS/Triton X-100 solution, 10 ml of elution buffer (10 mM glutathione and 10 mM Tris, pH 8.0) was added to the beads, and the supernatant containing GST-BAG-1 protein was recovered after 20 min at room temperature by centrifugation and dialyzed against PBS. Protein concentrations were estimated by Coomasie Blue staining of material in SDS-PAGE gels containing BSA standards.

Hsc70 Binding Assays. GST-Hsc70 (ATPase domain) and GST-CD40 (cytosolic domain) fusion proteins were produced and affinity-purified as described (5). Fusion proteins were then mixed at ~0.5–1.5 μg/μl of glutathione-Sepharose (packed volume) in binding buffer [10 mM HEPES (pH 7.5), 138 mM KCl, 2 mM EGTA, 5 mM $MgCl_2$, and 0.2% NP40 with 5% (w/v) BSA]. After washing the beads three times with the same solution to remove unbound GST fusion proteins, 5 μl of *in vitro* translation reactions in 95 μl of binding buffer were added to 15–20 μl of GST-beads, and the samples were nutated at 4°C for 2 h. Beads were washed three times in ice-cold binding buffer and resuspended in 20 μl of Laemmeli sample buffer, boiled, and analyzed by SDS-PAGE (12% gels). Gels were washed with ddH_2O and fixed in 10% acetic acid/25% isopropanol solution for 20 min, followed by 1.1 M sodium salicylate for 20 min, then dried and exposed to X-ray film.

***In vitro* Translations.** Proteins were translated *in vitro* in the presence or absence of [^{35}S]L-methionine (EASYTAG S.A.; ~1,000 Ci/mmol; New England Nuclear, Inc.) using the TNT lysate kit and T7 RNA polymerase with 1 μg of pcDNA3 or pSKII-based plasmids in a total volume of 50 μl, according to the manufacturer's recommendations (Promega, Inc.).

RNA Blot Analysis. Total cellular RNA was prepared from 5 × 10^7 cells using an acidic-phenol/guanidine thiocyanate method (22, 23). RNA (10 μg/lane) was size-fractionated by gel electrophoresis in 1% agarose gels containing glyoxal and then transferred to nylon membranes (Zetaprobe; BioRad, Inc.) by a semidry downward capillary method using alkaline transfer buffer (22), followed by UV cross-linking (2400 joules; Stratalinker; Stratagene, Inc.). Blots were prehybridized in 1% SDS, 1 M NaCl, and 10% dextran sulfate, at 60°C for 1 h, followed by hybridization in the same solution containing 100 μg/ml of denatured, sheared, salmon sperm DNA and ~2 ng/ml of ^{32}P-labeled probe, which was prepared by a random priming method (Boehringer-Mannheim, Inc.) using a gel-purified mouse BAG-1 cDNA SN245-9 (1). Blots were washed twice in 2× SSC (24) at ambient temperature for 5 min and then twice in 2× SSC with 1% SDS at 60°C for 30 min, and then finally in 0.1× SSC at room temperature for 10–60 min, before exposure to X-ray film (Kodak, Inc.) using intensifying screens at −80°C.

Subcellular Fractionations. Nuclear and nonnuclear fractions were prepared according to the method of Hennighausen and Lubom (24). Briefly, ~1–5 × 10^7 cells were washed twice in ice-cold PBS and resuspended on ice in 0.5 ml of homogenization buffer [10 mM HEPES (pH 7.2), 10 mM KCl, 1.5 mM $MgCl_2$, 0.4% NP40, 0.3 M sucrose, 0.1 mM EGTA, 0.5 mM DTT, 0.5 mM PMSF, 2.5 mM benzamidine, 10 μg/ml aprotinin, and 5 μg/ml leupeptin]. After disrupting cells with 10–20 strokes of a Dounce homogenizer using a B pestle and verifying complete lysis by phase-contrast microscopy, 0.1-ml aliquots of the lysate were centrifuged at 350 × *g* for 5 min at 4°C in a swinging-bucket rotor to pellet nuclei. The nuclei were then washed twice in the same buffer and finally resuspended in RIPA buffer (16). The postnuclear supernatant was cleared by centrifugation at 16,000 × *g* for 2–3 min before storing at −80°C. Fractions were normalized for either cell-equivalents or total protein content based on the bicinchoninic acid method (Pierce, Inc.) before SDS-PAGE/immunoblot assay.

Cell Transfections. Rat-1 fibroblasts were transfected by a calcium phosphate DNA precipitation method at ~70% confluence in 10-cm diameter dishes. The culture medium (10 ml of DMEM with 10% fetal bovine serum) was changed 4 h before transfection with 10 μg of plasmid DNA that had been resuspended in 438 μl of ddH_2O, supplemented with 62 μl of 2 M $CaCl_2$/10 mM HEPES (pH 5.8), and then added dropwise to 500 μl of 2× HBSS [40 mM HEPES (pH 7.05), 275 mM NaCl, 10 mM KCl, 1.4 mM Na_2HPO_4, and 12 mM glucose]. The DNA-calcium-phosphate precipitate was removed after 8–12 h and replaced with fresh medium.

HeLa cells were seeded at 7 × 10^5 per 60-mm plate on the day before transfections. Cells were transfected with a total of 3 μg of DNA (pEGFP-mBAG-1 in combination with either pRc/CMV or pRc/CMV/Bcl-2 at a 1:2 molar ratio) using 15 μg of lipofectin (Life Technologies, Inc.) and 3 ml of OPTI-MEM I (Life Technologies, Inc.). After 6 h, the cells were recovered by trypsinization and seeded into glass-bottomed culture dishes (MatTek Corp., Ashland, MA) and returned to culture in DMEM/10% serum medium for 2 days.

RESULTS

Production and Characterization of BAG-1 Monoclonal Antibodies: Identification of Several BAG-1 Isoforms in Human Tissues. Immunoblot analysis was undertaken using whole-cell lysates derived from a variety of human tissues using anti-huBAG-1 monoclonal antibodies. Detailed comparisons of three independent anti-human BAG-1 monoclonal antibodies (KS-6C8, KS-10B6, and KS-5A6) demonstrated essentially identical patterns of reactivity with proteins in these tissue lysates, although data are shown here only for the KS-6C8 antibody

(Fig. 1). The epitope on BAG-1 detected by KS-6C8 was mapped to residues 132–221, whereas KS-5A6 and KS-10B6 bound to residues 52–131, based on immunoblot analysis of a panel of GST-BAG-1 fusion proteins (see "Materials and Methods").

All three anti-BAG-1 antibodies detected several proteins in certain tissues, in addition to the anticipated ~36 kDa BAG-1 protein originally predicted from cDNA cloning. Ovary and testis, for example, contained a ~56–57 kDa isoform of BAG-1, as well as small amounts of an additional ~52–53 kDa protein (Fig. 1). Many tumor cell lines also contained these ~52–53 and ~56–57 kDa BAG-1 bands, in addition to the expected ~36 kDa BAG-1 protein (see below). Lysates derived from peripheral blood mononuclear cells and tonsils uniquely contained still other anti-BAG-1 immunoreactive bands of ~37–38 kDa, which may represent phosphorylated forms of the major ~36 kDa BAG-1 protein.[5] Note that in contrast to the larger ~52–57 kDa and ~37–38 kDa forms of BAG-1, the predicted ~36 kDa BAG-1 protein was ubiquitously present throughout most human tissues, although liver, colon, breast, and uterine myometrium contained comparatively little of this protein.

Immunoblot analysis of murine tissues similarly revealed widespread expression of a ~30 kDa protein corresponding to BAG-1 (Fig. 1*B*), indicating that this is by far the most abundant isoform of the protein *in vivo*. However, several mouse tumor cell lines contained a ~50 kDa anti-BAG-1 immunoreactive band, in addition to the ~30 kDa originally described isoform of BAG-1. Of note, the pattern of anti-BAG-1 immunoreactive bands was less complex in murine compared with human tissues (discussed below).

In contrast to the variety of BAG-1 proteins seen in tissues, BAG-1 mRNAs were homogeneous with only one species identified by Northern blotting. A survey of several tissues derived from mice, for example, revealed the presence of a single transcript of ~1.8 kbp (Fig. 2*A*). Note that all tissues tested contained BAG-1 mRNA, although liver had the least relative amounts of BAG-1 mRNA, which required longer exposures to clearly visualize. Human cell lines also contained a single BAG-1 mRNA of ≈1.9 kbp (Fig. 2*B* and data not shown).

BAG-1 Isoforms Arise by Alternative Translation Initiation Site Usage within a Common BAG-1 mRNA. The presence of ~52–57 kDa bands reacting with three different anti-BAG-1 monoclonal antibodies suggested the presence of isoforms of this protein that arise by alternative mRNA splicing. However, exhaustive efforts to clone cDNAs encoding alternative forms of human and mouse BAG-1 proved fruitless. Inspection of the longest human and murine BAG-1 cDNAs cloned previously in our laboratory revealed an absence of stop codons upstream of the predicted ORFs encoding the most prevalent isoform of the human and mouse BAG-1 proteins, estimated to be 230 and 219 amino acids in length, respectively. Moreover, an additional upstream and in-frame ATG codon was found in the human BAG-1 mRNA, which would extend the ORF by 44 amino acids, leading to production of a 274-amino acid protein (Fig. 3). Recently, it has been suggested that this longer isoform of the human BAG-1 protein is identical to RAP46, a protein that binds steroid hormone receptors (15, 16). However, an analogous ATG codon was not found in the murine BAG-1 cDNAs (Fig. 3), implying that additional mechanisms must exist for generating longer isoforms of the BAG-1 protein.

Although no in-frame ATG codons are found in murine BAG-1 cDNAs, three upstream and in-frame CTG codons are present at positions −408, −360, and −336 bp relative to the ATG start codon of the originally described ORF. Similarly, the region 5′ of the human BAG-1 ORF contains analogous CTG codons at positions −345, −297, and −273. CTG codons are occasionally used as an alternative to ATG for translation initiation in eukaryotic mRNAs (25, 26). Among these upstream, in-frame CUG codons, however, only the most 5′ CUGs in the predicted human and mouse BAG-1 mRNAs are within an optimal context for translation initiation, with purines at −3 and a guanosine (G) at +4 relative to the CUG (where the C is +1; Refs. 25 and 26). Genomic cloning confirmed the absence of introns between the previously described ORF and this 5′ region in the mouse *BAG-1* gene (not shown).

To explore the possibility that the murine BAG-1 cDNA containing this 5′-untranslated region where the CTG codons reside could encode both the usual 219-amino acid BAG-1 protein plus a longer protein that might account for the ~50 kDa form of mouse BAG-1 seen by immunoblot analysis of murine tissues, a mouse BAG-1 cDNA containing this 5′-untranslated region was subcloned downstream of the T7 RNA polymerase in pSKII and *in vitro* transcribed and translated using reticulocyte lysates. Comparisons were made with a mouse BAG-1 cDNA that contained the usual ORF but which lacked this 5′

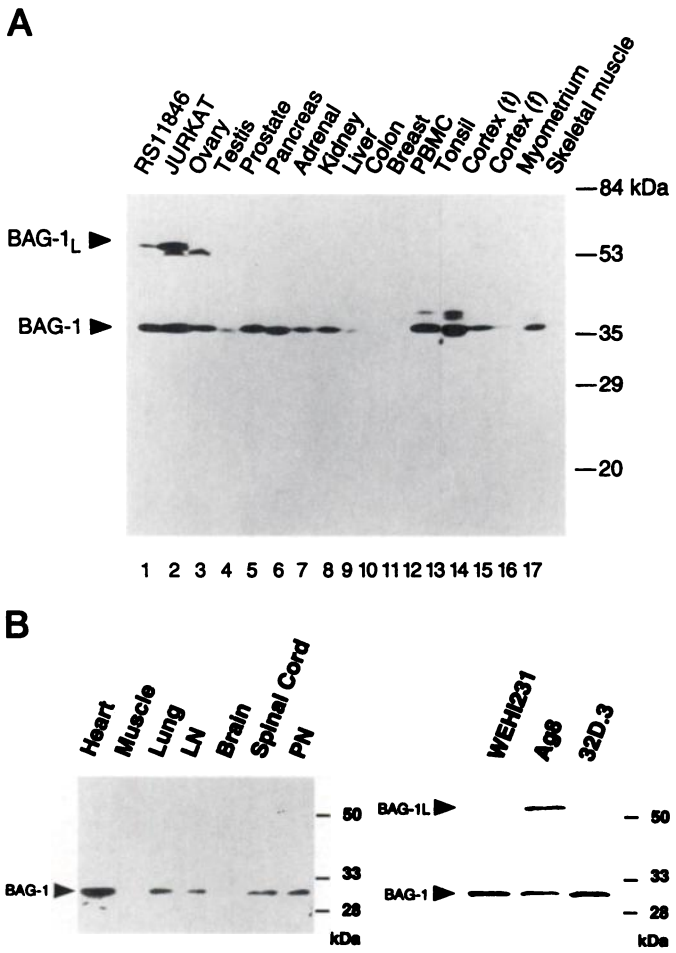

Fig. 1. Immunoblot analysis of BAG-1 proteins in tissues. In *A*, human tissue lysates were prepared and normalized for total protein content (50 μg/lane) before analysis by SDS-PAGE/immunoblot assay using the anti-human BAG-1 monoclonal antibody KS-6C8. Essentially identical results were obtained with two other independent monoclonal antibodies. *Arrowheads*, positions of the ~36-kDa BAG-1 and ~53–57-kDa higher molecular weight forms of BAG-1 proteins (*BAG-1L*). A ~38-kDa BAG-1 band seen in peripheral blood mononuclear cells (*PBMC*) and tonsil (*Lanes 13* and *14*) may represent a phosphorylated form BAG-1.[5] Both temporal (*t*) and frontal (*f*) brain cortex were analyzed (*Lanes 15* and *16*). Reprobing of the same blot with antibodies to other proteins such as tubulin and Bax confirmed that all samples contained intact proteins that appeared to be present in roughly equivalent amounts, with the exception of testis which was underloaded in this particular blot (not shown). In *B*, immunoblot results for a few representative mouse tissues (*left panel*) and mouse tumor cell lines (*right panel*) are presented. All samples were normalized for total protein content (50 μg/lane).

[5] Unpublished observations.

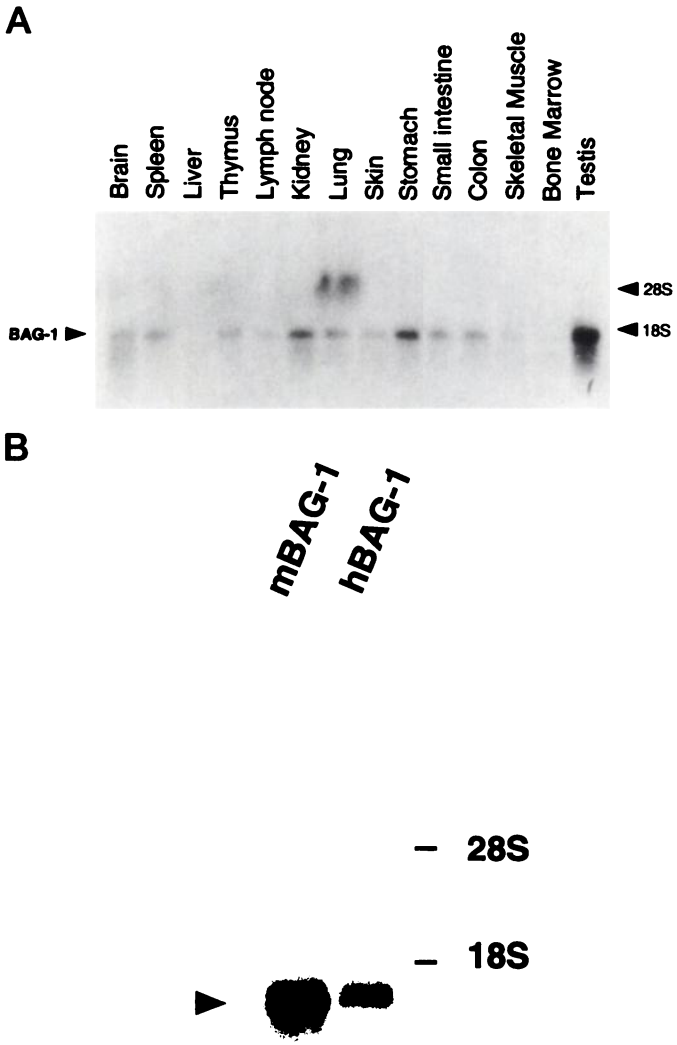

Fig. 2. RNA blot analysis of BAG-1 mRNA in tissues. Total cellular RNA was isolated from various mouse tissues (*A*) or from mouse S49.1 and human Jurkat T-cell leukemia cell lines (*B*) and analyzed by RNA blotting (20 μg/lane) using a ^{32}P-labeled muBAG-1 cDNA probe. Loading of approximately equivalent amounts of intact RNA was confirmed by visualization of the 28S and 18S rRNA bands in ethidium-stained gels (not shown). *Arrowheads*, positions of the ~1.8-kbp mouse and ~1.9-kbp human BAG-1 mRNAs.

region. The resulting *in vitro* translation products were then analyzed by SDS-PAGE/autoradiography (Fig. 4*A*) or by immunoblotting using a BAG-1 specific anti-peptide antiserum (not shown). As shown in Fig. 4*A*, *in vitro* translation of the mouse BAG-1 cDNA that lacked the upstream CTG containing region generated the expected ~29–30 kDa BAG-1 protein. In contrast, *in vitro* translation of the mouse BAG-1 cDNA that contained the 5′ upstream region resulted in the production of two BAG-1 immunoreactive proteins of 50 kDa and 29–30 kDa. No similar ^{35}S-labeled proteins or BAG-1 immunoreactive bands were observed when reticulocyte lysates were primed with pSK-II or pcDNA3 plasmids lacking BAG-1 cDNA inserts (not shown).

A similar result was obtained when human BAG-1 cDNAs were *in vitro* translated, except that the additional in-frame ATG codon generated another isoform of BAG-1, consistent with a recent report (14). For example, when a human BAG-1 cDNA, which contains both the originally described ORF plus the upstream in-frame ATG, was *in vitro* translated and the products were analyzed by either SDS-PAGE/autoradiography (Fig. 4*A*) or immunoblotting using an anti-BAG-1 monoclonal antibody (not shown), the anticipated ~36 kDa BAG-1 protein was observed as well as a longer ~52 kDa BAG-1 immunoreactive protein. Moreover, when a longer human BAG-1 cDNA was used that contains the 5′ in-frame CTG codons mentioned above, the predominant protein produced was a ~56–57 kDa BAG-1 immunoreactive band, with only very small amounts of translation initiation from the usual downstream ATG which generates the ~36 kDa BAG-1 protein and essentially none of the ~52 kDa protein predicted to arise from the 5′ in-frame ATG codon (Fig. 4*A*). Finally, comparisons were made with a human BAG-1 cDNA in which the first of the candidate noncanonical CTG start codons was mutated to ATG, thus forcing translation from this upstream site. As shown in Fig. 4*A*, *in vitro* translation of the human BAG-1 CTG→ATG mutant generated predominantly a ~56–57 kDa band, suggesting that the first CTG is the most likely site of translation initiation for generation of the ~56–57 kDa isoform of BAG-1. This ~56–57 kDa protein comigrated precisely in gels with the endogenous BAG-1 proteins seen in human tumor cell lines (see below). In contrast, the *in vitro* translation product derived from a BAG-1 cDNA in which the next CTG downstream was mutated to ATG resulted in a protein that migrated slightly faster in SDS-PAGE compared with the endogenous 56–57 kDa BAG-1 protein (not shown). None of the various ^{35}S-labeled proteins shown in Fig. 4 were observed when reticulocyte lysates were primed with control pSKII plasmid DNA, confirming the specificity of these results. We have designated the longer isoforms of human (~56–57 kDa) and mouse (~50 kDa) BAG-1 proteins that appear to arise from translation at noncanonical CTG codons as "BAG-1-long" (BAG-1L), and the intermediate length human BAG-1 protein which presumably arises from the in-frame upstream ATG codon as "BAG-1 medium" (BAG-1M).

To further verify that these proteins observed in the *in vitro* translation experiments corresponded to the BAG-1 immunoreactive species identified by immunoblot analysis of tissues, *in vitro* translated proteins were compared side-by-side in gels with the cell-derived BAG-1 proteins that either arise naturally in some cell lines or that were produced by gene transfection. For these experiments, a human BAG-1 cDNA that includes the 5′ upstream region where the CTG codons reside and the ORFs for BAG-1 and BAG-1M was *in vitro* translated, giving rise to a prominent ~56–57 kDa BAG-1L product and less abundant amounts of ~52 kDa BAG-1M and ~36 kDa BAG-1. These bands comigrated in SDS-PAGE with BAG-1 immunoreactive bands seen in some tumor cell lines such as Jurkat T-cell leukemia, which produces all three isoforms of BAG-1 (Fig. 4*B*). These same bands corresponding to BAG-1, BAG-1M, and BAG-1L were detected using all three of our anti-BAG-1 monoclonal antibodies raised against the ~36 kDa BAG-1 protein (data not shown).

The ability of a single BAG-1 cDNA to encode both the originally identified ~36 kDa BAG-1 protein and longer ~56–57 kDa BAG-1L isoform was confirmed by expressing in mammalian cells the same human BAG-1 cDNA that had been used for the *in vitro* transcription/translation experiments. For this purpose, the BAG-1 cDNA was subcloned downstream of the cytomegalovirus immediate early-region promoter in pcDNA-3, and this plasmid or the control pcDNA-3 plasmid was stably transfected into Rat-1 fibroblasts. Immunoblot analysis of lysates derived from these cells revealed the presence of two isoforms of BAG-1 having apparent molecular masses of ~36 kDa and ~56–57 kDa in the BAG-1-transfected Rat-1 cells but not in

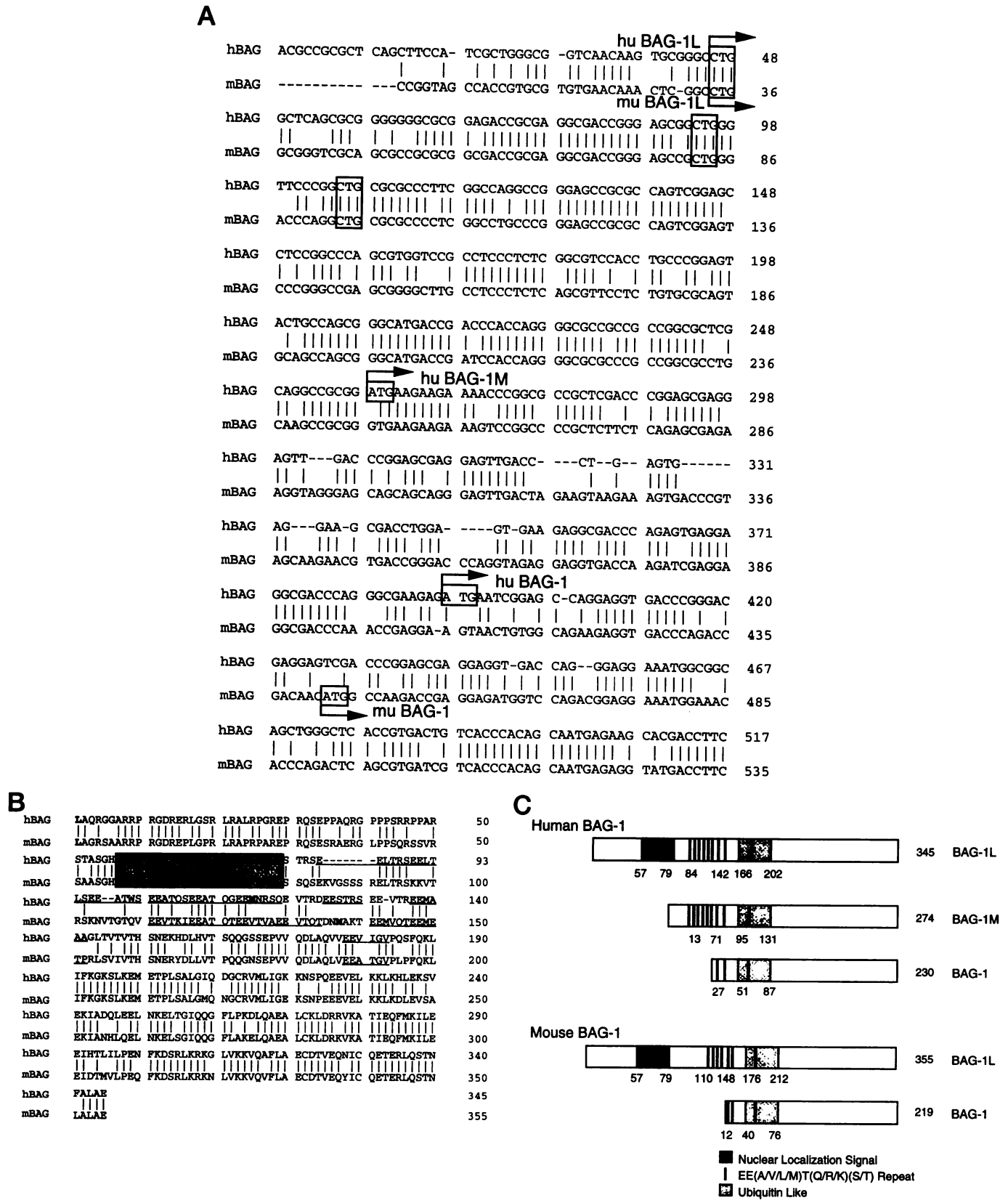

Fig. 3. Nucleotide and predicted amino acid sequences of human and mouse BAG-1 mRNAs and proteins. In *A*, a portion of the nucleotide sequences of human and mouse BAG-1 cDNAs are presented (submitted to GenBank). The locations of the predicted ATG start codons and the alternative upstream CUG codons are indicated in *boxes*. The CUG codon with the most favored context for translation initiation is indicated by an *arrow*. The two downstream CUGs have pyrimidines rather than the favored purines at positions −3 and/or +4 relative to the CUG (where C is +1). *B*, the predicted amino acid sequences of the human and mouse BAG-1L proteins are presented in single-letter code, assuming translation initiation from the most 5′ CUG codon. The methoniones corresponding to the AUG codon initiation sites are in *bold*. A basic region with similarity to NLS motifs is shaded. The six amino-acid EE motifs [most common sequence is E-E-(A/V/L/M)-T-(Q/R/K)-(S/T)] are *underlined*. In *C*, a schematic of the human and mouse BAG-1 isoforms is presented, illustrating the ubiquitin-like domain NLS and hexameric repeats (see "Discussion").

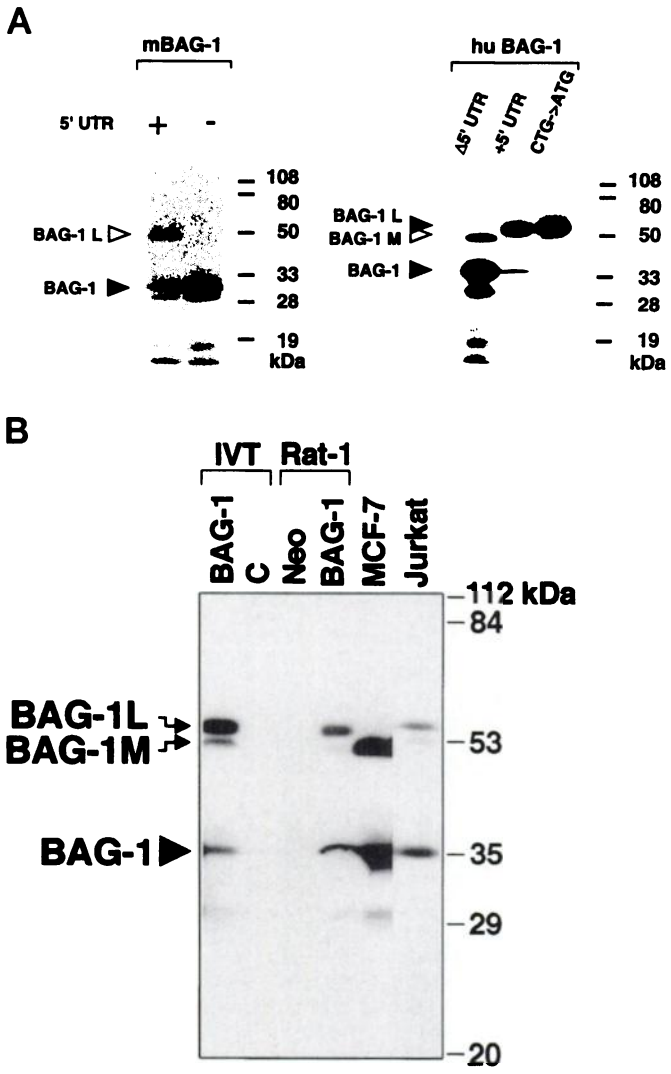

Fig. 4. The BAG-1L protein derives from use of noncanonical CTG codons for translation initiation. In *A*, *in vitro* translations were performed in the presence of [^{35}S]L-methionine using murine (*left panel*) and human (*right panel*) BAG-1 cDNAs that either contain or lack the 5′-untranslated region (*UTR*) where the CUG codons reside. The human BAG-1 cDNA encompasses position −345 bp to 690 bp relative to the ATG (A is +1) that initates the ORF encoding the shortest BAG-1 protein, whereas the murine BAG-1 cDNA encompasses positions −408 bp to 657 bp. The same human BAG-1 cDNA, but in which the 5′ most CUG codon was mutated to ATG, was also *in vitro* translated. Proteins were analyzed by SDS-PAGE/autoradiography. The BAG-1, BAG-1L, and BAG-1M proteins are indicated by *arrowheads*. In *B*, immunoblot analysis was performed using either *in vitro* translated proteins or lysates (50 μg/lane) derived from cells. *Lanes 1* and *2* represent reticulocyte lysates (3 μl) used for *in vitro* transcription/translation of either control pcDNA3 plasmid (*c*) without an insert or a huBAG-1 cDNA (pKK240) encoding nucleotides −390 to 880 bp relative to the AUG codon (A is 1+). *Lanes 3* and *4* are Rat-1 cells that had been stably transfected with either a control plasmid pcDNA-3 or pcDNA-3 containing the pKK241-1 huBAG-1 cDNA (−390 to 880 bp). Lysates were also included from MCF7 breast cancer cells stably transfected with a BAG-1 expression plasmid that produces both BAG-1M and BAG-1 but which lacks the upstream CTG required for BAG-1L (*Lane 5*) and from untransfected Jurkat T-cell leukemia cells which intrinsically express all three isoforms of BAG-1 (*Lane 6*). The blot was incubated with anti-huBAG-1 monoclonal antibody KS-6C8, followed by ECL-based detection. The positions of the BAG-1, BAG-1L, and BAG-1M proteins are indicated.

the control (Neo)-transfected cells. These two forms of BAG-1 detected in transfected Rat-1 cells comigrated in gels with the anti-BAG-1 immunoreactive bands seen in Jurkat and some other human cell lines (Fig. 4*B* and data not shown). The intermediate BAG-1M protein was not produced in these transfected Rat-1 cells. To demonstrate production of the BAG-1M protein in cells, MCF7 breast cancer cells were transfected with a BAG-1 cDNA containing the ORFs for BAG-1 and BAG-1M but lacking the 5′ region where the CTG codons reside. Deletion of the 5′ upstream region was empirically determined to allow for more efficient translation initiation from the downstream ATG codons. In these transfected MCF7 cells, abundant amounts of the ~52 kDa BAG-1M and ~36 kDa BAG-1 proteins were observed but not the longer BAG-1L protein (Fig. 4*B*).

Taken together, these data corroborate and extend recent observations (14) demonstrating that the human BAG-1 mRNA can potentially encode three isoforms having lengths of 345 (BAG-1L), 274 (BAG-1M), and 230 (BAG-1) amino acids, with BAG-1L arising from a noncanonical CUG and the BAG-1M and BAG-1 proteins arising from typical AUG codons. The cDNA cloning results presented here also provide evidence that the mouse BAG-1 mRNA can similarly encode two isoforms of 355 (BAG-1L) and 219 (BAG-1) amino acids in length (Fig. 3), with the longer of these arising from a noncanonical CUG codon.

BAG-1L and BAG-1M Proteins Retain Hsc70 Binding Activity. Recently, we reported that the shorter BAG-1 protein can bind to Hsp/Hsc70 family proteins and modulate their activities (5). We therefore explored whether the BAG-1L and BAG-1M variants of BAG-1 can also bind to molecular chaperones. For these experiments, a GST-fusion protein containing the ATP-binding domain of Hsc70 was tested for interactions *in vitro* with the BAG-1, BAG-1L, and BAG-1M proteins, which were produced by *in vitro* translation of BAG-1 cDNAs that either contained or lacked the region where the noncanonical CTG start codons reside. The COOH-terminal peptide-binding domain of Hsc70 was not included in the GST-fusion protein to avoid nonspecific association and because our previous experiments showed that BAG-1 binds directly to the ATP-binding domain

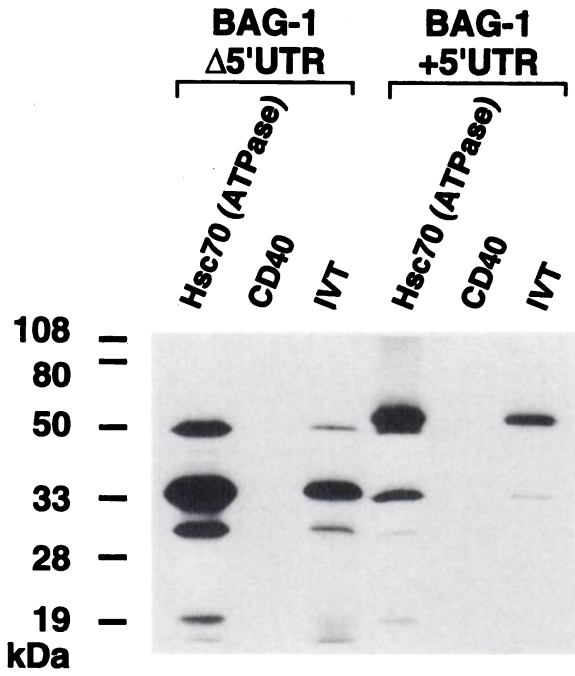

Fig. 5. Hsc70 binds to BAG-1, BAG-1L, and BAG-1M. Human BAG-1 cDNAs containing or lacking the region upstream of the originally identified ORF were *in vitro* translated (*IVT*) in the presence of [^{35}S]L-methionine, thus producing the BAG-1, BAG-1M, and BAG-1L proteins. The BAG-1 (*+5′UTR*) cDNA produces primarily BAG-1L, whereas the BAG-1 (*Δ5′UTR*) cDNA produces mostly BAG-1 along with some BAG-1M protein. IVT BAG-1 proteins were incubated with GST-Hsc70 (ATP-binding domain) or (as a negative control) GST-CD40 cytosolic domain immobilized on glutathione-Sepharose. After washing, proteins bound to beads were analyzed by SDS-PAGE/autoradiography. As a control, one-tenth the input volume of the IVT proteins was run directly in gels. Note that BAG-1, BAG-1M, and BAG-1L bind to GST-Hsc70 but not to GST-CD40. The small molecular weight proteins presumably represent partial degradation products of BAG-1 or translation initiation from internal AUG codons. These small proteins have not been detected *in vivo*, arising only in IVT experiments.

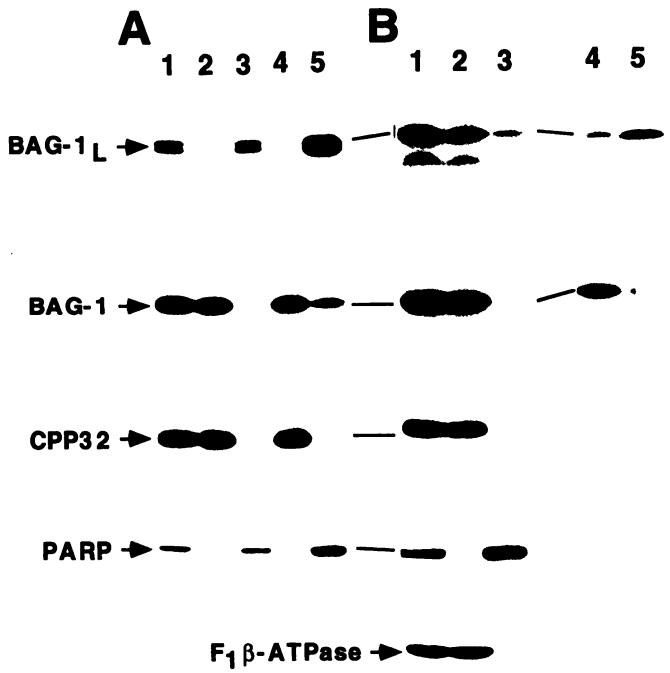

Fig. 6. Subcellular fractionation analysis of BAG-1 proteins. Nuclear and nonnuclear fractions were prepared from 267 prostate cancer (*A*) and Jurkat T-cell leukemia (*B*) cell lines. Lysates were normalized either for cell equivalents ($4\text{-}10^5$, *A*; 10^6, *B*) (*Lanes 1–3*) or for total protein content (50 μg/lane; *Lanes 4* and *5*). Whole-cell lysates were included for comparison (*Lane 1*). With cytosolic (*Lanes 2, 4*) and nuclear (*Lanes 3, 5*) extracts. After SDS-PAGE and transfer to nitrocellulose, blots were sequentially probed with antibodies specific for BAG-1, the cytosolic protein CPP32 (caspase-3), the nuclear protein poly(ADP-ribose) polymerase (*PARP*), or the mitochondrial protein $F_1$1-β-ATPase using a multiple antigen detection method (17). The positions of the BAG-1 and BAG-1L proteins are indicated. Jurkat T-cells (*B*) also contain some BAG-1M.

of Hsp70 and Hsc70 (5). As shown in Fig. 5, the BAG-1L, BAG-1M, and BAG-1 proteins all bound to GST-Hsc70(ATP domain) but not to a control GST fusion containing the cytosolic domain of CD40. Similar results were obtained in coimmunoprecepitation assays using lysates from cells that endogenously contain BAG-1, BAG-1M, and BAG-1L (not shown). Thus, BAG-1 and its variants BAG-1L and BAG-1M can all interact with Hsc70.

BAG-1 Proteins Can Reside in the Nucleus. The additional NH_2-terminal region found in both the human and mouse BAG-1 proteins is predicted to contain a basic stretch of amino acids resembling NLSs such as that found in nucleoplasmin (Fig. 3*B*; Refs. 27 and 28). We therefore explored the subcellular locations of these proteins by preparing nuclear and nonnuclear fractions from a human leukemia line, Jurkat, and a prostate cancer line 267 that contain relatively high endogenous levels of the BAG-1 and BAG-1L proteins. Jurkat T-cells also contain lower but detectable levels of BAG-1M.

In 267 prostate cancer cells, the shorter ~36 kDa BAG-1 protein was located predominantly in the nonnuclear fraction with only a small proportion of this observed in the nucleus (Fig. 6*A*). In contrast, the BAG-1L protein was found predominantly in the nuclear fraction, regardless of whether samples were normalized for cell equivalents or total protein content (Fig. 6*A*). In contrast, in Jurkat T-cells, most of the BAG-1, BAG-1L, and BAG-1M proteins resided in the nonnuclear fraction in Jurkat T-cells, as determined by immunoblot analysis where cell equivalents were used for sample normalization (Fig. 6*B*, *Lanes 1–3*). However, some of the BAG-1L protein was also detected in the nuclear fraction by immunoblot analysis. Reprobing the same blot with antibodies specific for a cytosolic protein (CPP32), a nuclear protein (PARP), and a mitochondrial protein (F1-β-ATPase) confirmed the purity of these subcellular fractions (Fig. 6). When the Jurkat nuclear and nonnuclear fractions were normalized for total protein content (Fig. 6*B*, *Lanes 4* and *5*), a reciprocal relation was observed between the relative amounts of BAG-1 and BAG-1L in these subcellular fractions, with higher levels of BAG-1 in the nonnuclear compared with the nuclear compartment and conversely higher levels of BAG-1L in the nuclear than the nonnuclear fractions. These findings therefore suggest that the BAG-1L protein is commonly located in the nucleus, whereas the shorter BAG-1 protein tends to be nonnuclear. Note however that some of the shorter ~36 kDa BAG-1 protein was also present in the nuclear fraction. Consequently, these data argue that BAG-1 and BAG-1L can reside in either the cytosol or the nucleus, although they may have preferences for one location or the other.

To further evaluate the intracellular locations of the BAG-1 and BAG-1L proteins, we used confocal immunofluorescence microscopy methods. In Rat-1a cells that had been transfected with a human BAG-1 cDNA and that expressed roughly equivalent amounts of the 56–57 kDa BAG-1L and 36 kDa BAG-1 proteins (see Fig. 4*B*), immunofluorescence-based detection of the human BAG-1 protein revealed localization predominantly in the nucleus (Fig. 7). In contrast, expression of human or murine BAG-1 plasmids capable of producing only the shorter BAG-1 protein in several types of cells generally resulted in a predominantly cytosolic distribution (not shown). Taken together, these observations derived from subcellular fractionation and immunofluorescence confocal microscopy confirm that BAG-1 proteins can reside in either the nucleus or the cytosol, with the BAG-1L protein apparently having a preference for the nucleus. However, the cellular background in which BAG-1 is expressed can influence whether it resides primarily in the cytosol or is also found in the nucleus.

Immunolocalization of BAG-1 Proteins in Human and Mouse Tissues by Immunohistochemistry. Using the anti-BAG-1 monoclonal antibody KS-6C8, an immunohistochemical analysis of BAG-1 expression in essentially all normal adult human tissues was performed. Although only the data for the KS-6C8 anti-human BAG-1 monoclonal, major portions of the immunostaining results were confirmed by use of the KS-10B6 and KS-5A6 anti-human BAG-1 monoclonals. All of these monoclonal antibodies react with the

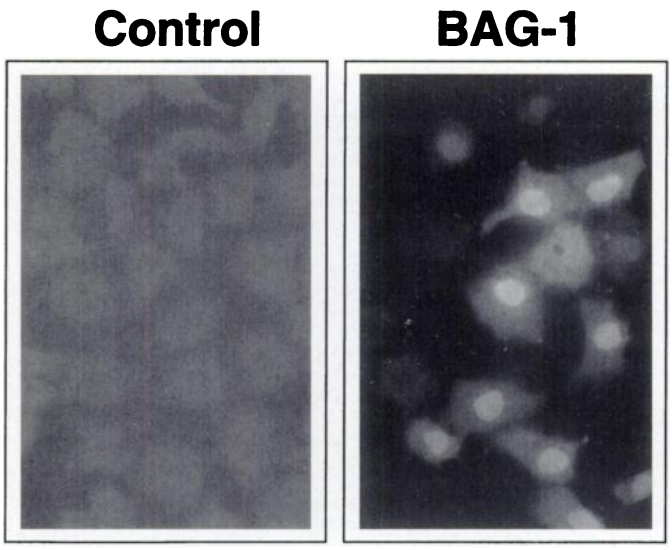

Fig. 7. Confocal immunofluorescence analysis of intracellular distribution of BAG-1 proteins demonstrates nuclear location. Rat-1a cells, which had been stably tranfected with a huBAG-1 cDNA (encompassing nucleotides −390 to 880 bp relative to the AUG), were analyzed for huBAG-1 protein expression by immunofluorescence assay. After fixation, cells were incubated with either a mIgG1 control (*left*) or the anti-huBAG-1 monoclonal antibody KS-6C8, followed by a FITC-confugated secondary antibody.

Table 1 *Summary of immunohistochemical analysis of in vivo BAG-1 expression in normal tissues*

Organ/Tissue	Structure/Cell type	Intensity[a]
Skin		
Epidermis	Keratinocytes	
Stratum basale	Basal cell layer	1–3+c
Stratum spinosum	Spinous layer	2+d
Stratum granulosum	Granular layer	1–2+b
Stratum corneum	Cornified layer	0
Dermis		
Connective stroma	Fibroblasts	0–2+b
Sweat gland	Epithelium	2–3+b
Sabaceous gland	Epithelium	1–2+b
Musculoskeletal system		
Skeleton		
Cartilage	Chondrocytes	1–3+d
	Fibroblasts	0–1+b
Bone	Osteocytes	1–3+b
	Osteoclasts	1+b
Striated muscles	Muscle fibers	1–2+a,c
Cardiovascular system		
Heart		
Myocardium	Myocytes	1–2+d
	Fibroblasts	0–1+b
	Capillary endothelium	0
Arteries	Endothelial cells	0
	Smooth muscle cells	0–2+b
	Fibroblasts	0–1+b
Respiratory system		
Trachea		
Epithelium (pseudostratified columnar)		
	Basal cell layer	0–1+b
	Luminal cell layer	2–3+a
Submucosa	Fibroblasts	0–1+b
	Smooth muscle cells	0–1+b
	Sero-mucous glands	0
Cartilage	Chondrocytes	0–2+d
Lung		
Bronchi	Pseudostratified or simple columnar epithelium	2–3+a
Alveoli	Type I pneumocytes	0
	Type II pneumocytes	0
	Alveolar macrophages	2–3+a
Alimentary tract		
Salivary gland (submandibular gland)		
Secretory gland acini	Serous cells	0
	Mucous cells	0
	Salivary duct epithelium	1–3+a
Tongue/Esophagus		
Stratified squamous epithelium	Basal cell layer	0–1+c
	Spinous layer	1–2+d
	Granular layer	0–1+b
Muscularis externa	Smooth muscle cells	0–1+b
Stomach		
Cardiac region	Gastric pits/foveolar cells	2–3+d
	Cardiac glands/mucoid cells	0–3+a,c
Submucosal plexus (Meissner's plexus)	Ganglion cells	1+d
	Smooth muscle cells	0–1+b
Small intestine	Absorptive epithelium	1+d
	Paneth cells	0–1+b
Colon	Absorptive cells	1–2+b
	Goblet/mucous cells	0
Myenteric plexus (Auerbach's plexus)	Ganglion cells	0–1+d
Liver	Hepatocytes	1–3+a
	Sinusoidal endothelium	0–1+b
	Bile duct epithelium	2–3+a
Pancreas		
Exocrine	Acinar cells	2–3+a
	Ductal epithelium	1–2+b
Endocrine: Islets of Langerhans	A cells	2–3+a
	B cells	0–1+a
Urinary system		
Kidney		
Glomeruli	Mesangial cells	0
Bowman's capsule	Parietal layer/podocytes	0
	Visceral layer/squamous epithelium	0
Collecting tubules	Proximal convoluted tubules	0–1+d
	Loop of Henle, thin limb	1–2+a,d
	Distal convoluted tubules	2–3+a
Collecting ducts	Epithelial cells	1–3+a
Urinary bladder	Transitional epithelium	0–2+a
	Smooth muscle cells	0–1+b
Reproductive systems		
Male		
Testis	Leydig cells	0
Seminiferous tubules	Sertoli cells	0–3+b
	Spermatogonia	0–1+b
	Spermatocytes	0
	Spermatids	0
	Spermatozoa	0–3+d
Vas deferens	Pseudostratified columnar epithelium	0–1+b
Prostate		
Tubuloalveolar glands	Basal cells	1–3+d
	Luminal secretory cells	0–3+a
Fibromuscular stroma	Smooth muscle cells	0–1+b
	Fibroblasts	0–1+b
Female		
Uterus		
Endometrium	Columnar epithelium	0–3+a,c
	Stromal cells	0–1+b
Myometrium	Smooth muscle cells	0–1+b
Ovary		
Primordial/primary follicle	Oocytes	nf
	Follicular cells	0
Secondary follicle	Granulosa cells	0
	Theca internal cells	1+b
	Theca external cells	1+b
Corpus luteum	Granulosa lutein cells	0–1+b
	Theca lutein cells	0–2+d
Oviduct (Fallopian tube)		
Tunica mucosa	Ciliated columnar epithelium	2–3+a
	Secretory cells	0
Tunica muscularis	Smooth muscle cells	0–1+b
Mammary gland		
Tubuloalveolar glands	Cuboidal/columnar epithelium	1–3+d
Lactiferous ducts	Columnar epithelium	1–3+d
	Myoepithelial cells	0
Stroma	Fibroblasts	0–1+b
Hematolymphoid system		
Peripheral blood	Granulocytes	0–3+d
	Monocytes	0–2+b
	Lymphocytes	0
	Erythrocytes	0
Bone marrow	Erythroid precursors	0–1+b
	Myeloid precursors	0–1+b
	Megakaryocytes	2–3+c
	Mature neutrophils	1–3+d
	Plasma cells	0–1+d
	Monocytes	0–2+b
Thymus		
Cortex	Cortical thymocytes	0–1+b
	Macrophages (dendritic interdigitating cells)	0
Medulla	Epithelioreticular cells	1–3+b
	Hassall's corpuscles	0–2+b
	Medullary thymocytes	0–1+b
Tonsil/Lymph nodes		
Germinal center	Large noncleaved cells	0
	Small noncleaved cells	0
	Small cleaved cells	0
	Follicular dendritic cells	0
	Macrophages	1–3+a
Mantle zone	Lymphocytes	0
Interfollicular region	Small T-cells	0
	Large transformed cells	0
	Sinus histiocytes	0–1b
	Plasma cells/reactive	1–2+d
Spleen		
Periarteriolar sheets	B-lymphocytes	0
Marginal zone	T-lymphocytes	0
Interfollicular cells	Granulocytes	1–3+d
	Erythrocytes	0
Venous sinsues	Endothelium	1–3+a
Central nervous system		
Cortex and basal ganglia		
Gray matter	Normal neurons	0–3+d
	Axons	1–2+b
	Neuropil	0–1+b
White matter	Myelin sheath	0
Neuroglia	Astrocytes	0–3+a
	Oligodendroglia	0
Microglia	Resting cells	0
	Activated cells	0

Table 1 *Continued*

Organ/Tissue	Structure/Cell type	Intensity[a]
Ependyma	Ependymal cells	1–2+b
Leptomeninges	Arachnoid epithelium	0
Choroid plexus	Epithelium	0
Cerebellum		
Cortex	Purkinje cells	1–2+d
	Granular cells	0
	Golgi cells	0
Molecular layer	Stellate and basket cells	0
	Purkinje cell dendrites	0–1+b
	Astrocytes (Bergman glia)	2–3+a
Medulla	Dentate nucleus	0–1+d
	Myelin fibers	0
Spinal cord		
White matter	Axons	0–1+b
	Myelin sheath	0
Gray matter	Ventral horn motoneurons	1–3+d
	Dorsal horn sensory neurons	0–1+b
	Neuro-pil	0–1+b
Central channel	Epen-pil	1+b
Peripheral nervous system		
Dorsal root and cranial nerve ganglia	Ganglion cells	0–3+d
	Satellite cells	0
	Schwann cells	0
	Fibroblasts	0
Autonomic ganglia	Ganglion cells	0–3+d
	Satellite cells	0
	Schwann cells	0
	Fibroblasts	0
Peripheral nerve	Axons	1–2+b
	Myelin sheath	0
Endocrine system		
Thyroid	Follicle cells	0–1+b
Adrenal		
Cortex	Zona glomerulosa	0–1+b
	Zona fasciculata	0–2+b
	Zona reticularis	0–2+b
Medulla	Chromaffin cells	2–3+c

[a] Immunohistochemical analysis of *in vivo* patterns of BAG-1 expression was performed for both human and mouse tissues. Results were scored according to intensity of immunostaining as: 0, negative; 1, weakly positive; 2, moderate; and 3, strong. The intracellular locations of BAG-1 immunostaining varied as indicated: a, organellar/mitochondrial pattern of expression; b, cytosolic; c, nuclear; and d, both nuclear and organellar/cytosolic pattern of expression. nf, not found.

BAG-1, BAG-1L, and BAG-1M proteins.[5] Moreover, immunohistochemical analysis was also performed for murine tissues using an anti-peptide polyclonal antiserum that is specific for residues 26–45 of the mouse BAG-1 protein (1), yielding similar results.

Table 1 summarizes the results, and Fig. 8 provides some of the more salient examples of BAG-1 immunoreactivity in normal tissues. A few of these results are commented upon here. Three subcellular patterns of BAG-1 immunostaining were identified, existing either individually or in combinations depending on the particular type of cell. These consisted of: (*a*) nuclear; (*b*) diffuse cytosolic; and (*c*) punctate cytosolic staining typical of association with organelles.

In the epidermis, cytosolic BAG-1 immunostaining was present throughout all the sublayers of keratinocytes (Fig. 8.1). The basal cell layer of cells, however, also contained nuclear BAG-1 immunostaining. Thus, the subcellular distribution of BAG-1 appears to change during differentiation of these epithelial cells, with loss of BAG-1 from the nuclei occurring as the cells differentiate and migrate toward the body surface. Combinations of diffuse cytosolic and nuclear BAG-1 immunostaining were also seen in chondrocytes (Fig. 8.3), cardiac myocytes (Fig. 8.4), colonic enterocytes (Fig. 8.10), bladder urothelium (Fig. 8.17), spermatogonia of the testis (Fig. 8.21), and mammary epithelial cells (Fig. 8.22). In some other types of cells, however, predominantly nuclear BAG-1 immunostaining with relatively little or no cytosolic staining was observed in the cells of the gastric glands (Fig. 8.7 and 8.8), intestinal epithelium (Fig. 8.9), corpus luteum of the ovary (Fig. 8.23), megakaryocytes in the bone marrow (Fig. 8.26), cortical and spinal cord neurons (Fig. 8.28 and 8.29), and adrenal chromaffin cells (Fig. 8.30 and 8.31).

Coarse, cytosolic granules of BAG-1 immunostaining were evident in several types of cells, sometimes with a perinuclear distribution, either alone or in combination with nuclear immunostaining, diffuse cytosolic staining, or both. Among the cells with organellar-like staining were cardiac myocytes (Fig. 8.4), bronchial epithelial cells (Fig. 8.5), alveolar macrophages (Fig. 8.6), exocrine pancreas (Fig. 8.11), renal collecting duct epithelium (Fig. 8.14), bladder epithelial cells (Fig. 8.18), and thymic epithelial cells (Fig. 8.24).

Analysis of this organellar immunostaining pattern at higher magnification revealed association of BAG-1 with what may be mitochondria (Fig. 9). In many cases, cross-sections through these organelles were obtained, demonstrating BAG-1 immunostaining around the circumference, thus producing a donut-like appearance. Similar observations were made by laser scanning microscopic analysis of these BAG-1-immunostained tissue sections (Fig. 9*F*). These results are highly reminescent of previous studies of Bcl-2 subcellular distribution using the same methods (21).

A few observations concerning the levels and locations of BAG-1 protein deserve comment: (*a*) the location of BAG-1 in some types of cells may be under dynamic regulation. Evidence for this comes, for example, from comparisons of BAG-1 immunostaining in prostates derived from several individuals, where either the mitochondrial or nuclear patterns prevailed depending on the specimen (not shown) and from the epidermis where BAG-1 appeared to move from a nuclear to a cytosolic location during differentiation of keratinocytes (Fig. 8.1); and (*b*) the intensity of BAG-1 immunostaining varied within some types of cells during their differentiation. For instance, BAG-1 immunostaining increased in intensity along the crypt-villus axis in the colon and small intestine, implying that BAG-1 protein levels become elevated as these cells differentiate and migrate toward the lumen of the bowel (Fig. 8.10). BAG-1 immunostaining was also strikingly up-regulated during differentiation of bladder epithelial cells and down-regulated during differentiation of prostate epithelium.

Bcl-2 Targets BAG-1 to Intracellular Membranes and Organelles. The immunohistochemical analysis of BAG-1 protein in tissues suggested that this protein can be associated with intracellular organelles, possibly mitochondria, in some types of cells. To explore whether expression of the integral membrane protein Bcl-2 can cause a relocation of BAG-1 to the intracellular membranes where it resides, a GFP-BAG-1 fusion protein was expressed in HeLa cells by transient transfection, with or without Bcl-2. As shown in Fig. 10 (left panels), when expressed by itself, the GFP-BAG-1 protein was diffusely distributed through the cytosol of HeLa cells. In contrast, coexpression of GFP-BAG-1 with Bcl-2 caused a portion of the GFP-BAG-1 to associate with what appeared to be the nuclear envelope and perinuclear membranes as well as punctate cytosolic structures suggestive of mitochondria. Because the Bcl-2 protein exhibits a similar distribution in cells (21), we conclude that the intracellular location of the BAG-1 protein can be modulated by Bcl-2.

Analysis of BAG-1 Expression in Human Tumor Cell Lines. To preliminarily explore the expression of BAG-1 in cancers, an immunoblot analysis was performed using the National Cancer Institute screening panel of 60 human tumor cell lines. Because prostate cancers are underrepresented in this screening panel, the analysis was supplemented with an additional five human prostate cancer cell lines. An additional B-cell lymphoma line (RS11846) and a T-cell leukemia Jurkat were also included. For these experiments, whole-cell lysates were prepared from tumor lines and normalized for total protein content before SDS-PAGE/immunoblot assay. Results were scored for each of the three forms of BAG-1 (BAG-1, BAG-1L, and BAG-

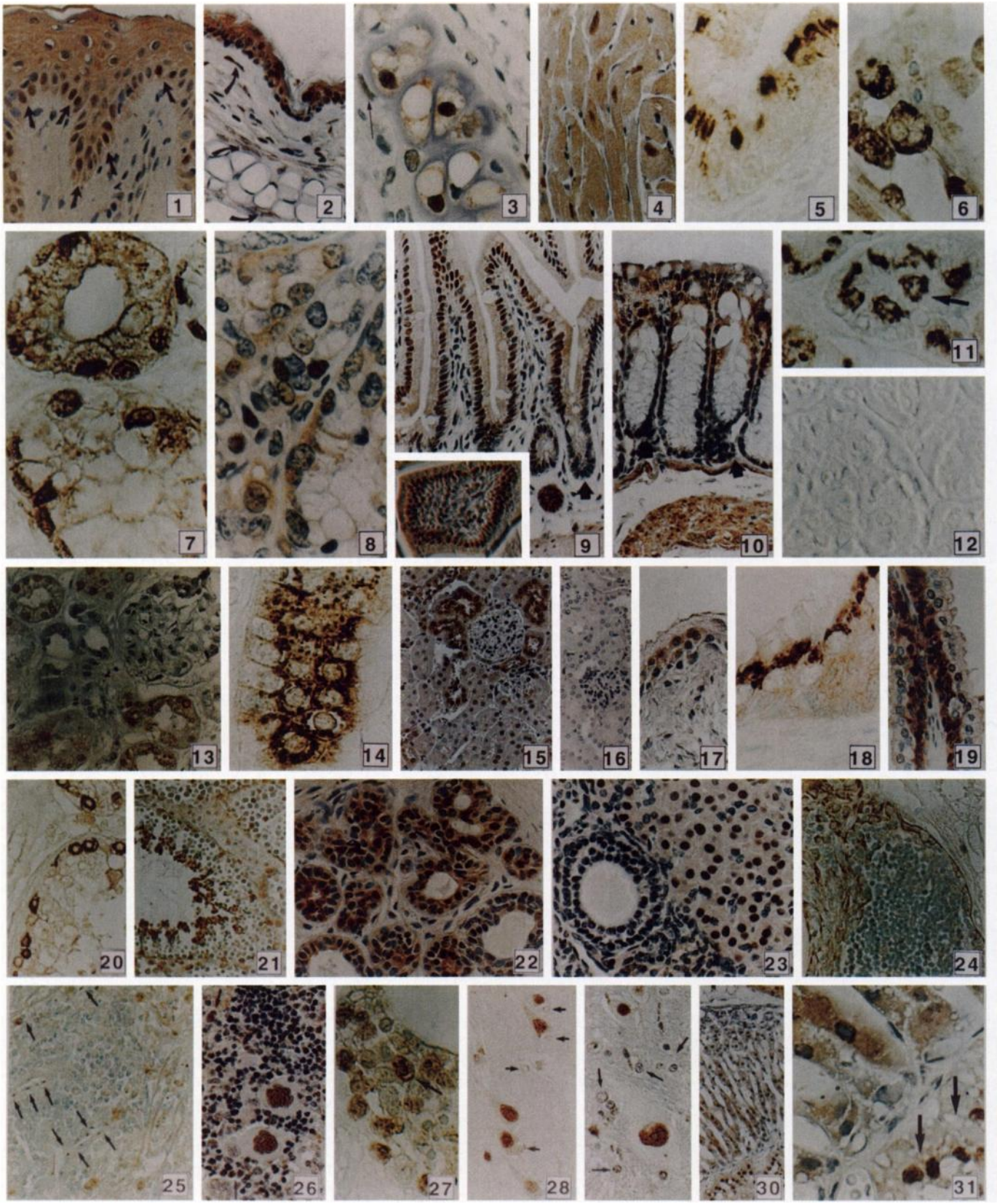

Fig. 8. Immunohistochemical analysis of BAG-1 expression *in vivo*. Representative BAG-1 immunostaining results are presented, showing some examples from both human and mouse tissues and representing 31 color photomicrographs taken with a 35-mm camera. Counterstaining of nuclei was performed with hexatoxylin, unless otherwise noted. *1*, human epidermis stained with KS6C8 demonstrating predominantly cytoplasmic immunoreactivity in all layers but nuclear BAG-1 in the basal cells lining the basement membranes (*arrows*); ×400. *2*, mouse epidermis from skin overlying the tail immunostained with anti-BAG-1 polyclonal antiserum, showing strong cytoplasmic and moderate nuclear BAG-1 immunoreactivity in keratinocytes in all layers of the epithelium. In the dermis below, faint cytoplasmic staining in fibroblasts and nuclear staining in perichondrial cells is present (*arrows*); ×200. *3*, cartilage from mouse, demonstrating strong nuclear and cytoplasmic BAG-1 immunostaining in chondrocytes. *Arrows*, immunopositive nuclei of cells in perichondrium; ×1000. *4*, mouse myocardium, showing cytosolic BAG-1 immunoreactivity, associated apparently with organelles, and nuclear BAG-1 expression; ×400. *5*, human bronchial epithelium, demonstrating intense BAG-1 immunostaining in a peri- or supranuclear distribution and having a clear granular pattern indicative of organella association (methylgreen counterstain). Faint diffuse cytoplasmic BAG-1 immunostaining is also present; ×1000. *6*, human alveolar macrophages exhibiting intense organellar-like BAG-1

1M), using a semiquantitative method that involved use of an internal control cell line to standardize results. As summarized in Table 2, the ~36 kDa BAG-1 protein was consistently the most abundant form of BAG-1 expressed in tumors. Among the tumor types with consistently higher relative levels of 36-kDa BAG-1 protein were breast, colon, and leukemia cell lines, although a variety of other types of tumor lines also expressed high levels of BAG-1 on a more variable basis. In contrast, the presence of the BAG-1L and BAG-1M proteins was highly variable. Prostate cancer, breast cancer, and leukemia cell lines were the most consistent expressors of BAG-1L, with seven of seven prostate, seven of eight breast, and four of five leukemia cell lines containing immunodetectable levels of this protein.

DISCUSSION

In this report, we explored the patterns of expression and intracellular distributions of the BAG-1 protein *in vivo* and in cultured cell lines. These data provide evidence that BAG-1 mRNAs and proteins are widely expressed *in vivo*, with the major form of BAG-1 protein representing the originally reported ~30 kDa mouse BAG-1 protein and a ~36 kDa human BAG-1 protein. The human and mouse BAG-1 proteins are predicted to be 230 and 219 amino acids in length, as deduced from cDNA cloning (1, 13), which coincides with proteins of ~26 kDa and ~25 kDa. Characterization of the BAG-1 protein by ultracentrifugation equilibrium sedimentation confirms this molecular mass.[5] However, like GrpE (29), molecular modeling and gel-sieve chromatography analysis suggest that BAG-1 is an elongated, rod-like molecule,[6] thus potentially accounting for its anomalous migration in SDS-PAGE. Moreover, both the human and mouse BAG-1 proteins are acidic (calculated pI of ~5.0 for human and ~4.8 for mouse) and thus may bind less SDS per unit mass, causing them to migrate slower in SDS-polyacrylamide gels than expected.

In addition to the originally described BAG-1 protein, we present evidence here that an additional generally less abundant form of BAG-1 can arise, most likely as a result of use of noncanonical CTG codons within BAG-1 mRNAs. Recent studies of human BAG-1 cDNAs by Packham *et al.* (14) also support this idea but lacked definitive evidence for an analogous configuration for murine BAG-1 cDNAs. Numerous studies have documented the ability of CUG codons to serve as alternatives to AUG for translation initiation, provided they are found within the proper sequence context (see for example Refs. 22 and 23). Based on predictions from cDNA cloning, the human and mouse BAG-1L proteins are expected to be 345 and 355 amino acids in length, respectively, assuming that the first of the available in-frame CTGs are used for translation initiation. Unlike the human BAG-1 cDNA, sequencing of murine BAG-1 cDNAs failed to reveal an in-frame upstream AUG codon that would give rise to a protein analogous to BAG-1M. Consistent with these DNA sequencing data, *in vitro* translation experiments resulted in the production of three isoforms of BAG-1 when the human cDNA was used compared with only two with the murine BAG-1 cDNA. It remains to be determined whether this species-specific difference is of functional importance, but immunoblot analysis of human tissues and multiple tumor cell lines indicated that BAG-1M (also known as RAP46) is by far the least abundant of the BAG-1 isoforms.

The originally described human and mouse BAG-1 proteins contain three copies of a 6-amino acid motif containing glutamic acid diamino acid (Glu-Glu) resides within their NH_2-terminal regions. The NH_2-terminal extensions present within the BAG-1L proteins of humans and mice add another six copies of this hexameric motif, for a total of nine copies. Although the function of this 6-amino acid motif is presently unknown, the preferred sequence is E-E-(A/V/L/M)-T-(Q/R/K)-(S/T). When this 6-amino acid motif is present in tandem copies, as is often the case in both huBAG-1 and muBAG-1, a consensus site for phosphorylation by creatine kinase-2 (T-R/Q-S-E) is generated. The first ~50 amino acids of the human and mouse BAG-1L proteins are also predicted to be proline rich. Moreover, in both the human and mouse BAG-1L proteins, this proline-rich region is followed by a stretch of basic residues resembling but not sharing perfect homology with NLSs (27, 28). Consistent with this idea, subcellular fractionation experiments and immunofluorescence confocal microscopy demonstrated the presence of BAG-1L within the nuclear compartment of at least some types of cells. The strong amino acid sequence homology shared by the human and mouse BAG-1 proteins within the NH_2-terminal domain created by translation from CUG codons implies an evolutionarily conserved purpose for this domain.

Comparison of the organization of mRNAs encoding bFGF reveals

[6] J. Stuart, D. Myszki, L. Joss, R. Mitchell, S. MacDonald, S. Takayama, Z. Xien, J. C. Reed, and K. Ely. Characterization of BAG-1 interactions with HSC70 molecular chaperones, submitted for publication.

immunostaining in their cytoplasm (methyl green counterstain); ×1000. *7* and *8*, human and mouse stomach, respectively, showing scattered cells within the gastric glands that contain strong nuclear BAG-1 immunostaining; ×1000. Human stomach was counterstained with methyl green (*panel 7*) to better demonstrate nuclear immunopositivity. *9*, murine small intestine demonstrating strong nuclear BAG-1 immunostaining in many of the enterocytes lining the surface of the villi. Note that the proportion of cells with nuclear immunopositivity increases toward the tip of villi (*arrow* points to base of villi where the BAG-1 immunopositive cells are more scarce; ×200. *Inset*, cross-section through a villus at higher magnification; ×400. *10*, colon from mouse, showing BAG-1 immunostaining associated with both nuclei and cytosol. The intensity of BAG-1 immunostaining appears to be greater within the epithelial cells at the apex of the crypts at the luminal surface and lower in the cells located in the bases of the crypts (*arrow*); ×200. *11*, human exocrine pancreas, demonstrating cells with perinuclear organellar-like BAG-1 immunostaining pattern that were counterstained with methyl green; ×1000. *12*, as a control, an adjacent section from the same pancreas was subjected to the immunostaining procedure using anti-BAG-1 monoclonal that had been preabsorbed with GST-BAG-1 fusion protein; ×1000. *13* and *14*, human kidney demonstrating immunonegative glomerulus but strong nuclear immunopositivity in the epithelial cells of proximal and distal convoluted tubules, with only faint cytoplasmic staining (*panel 13*; ×200); and strong cytosolic organellar-like BAG-1 immunostaining in collecting duct epithelium counterstained with methyl green (*panel 14*; ×1000), respectively. *15* and *16*, murine kidney showing same patterns of cell type specificity and intracellular location of BAG-1 immunostaining as observed in humans (*panel 15*; ×150) and demonstrating specificity by preadsorption of anti-muBAG-1 polyclonal antiserum (1735) with muBAG-1 26–45 peptide (*panel 16*; ×100). *17*, bladder urothelium of mouse with BAG-1 immunopositive cells in the subluminal layer with strong perinuclear immunostaining along with weaker diffuse nuclear and cytoplasmic immunoreactivity; ×200. *18*, human bladder transitional epithelium lining the human prostatic sinus with coarse granular cytoplasmic BAG-1 immunostaining of organelles and methylgreen counterstaining of nuclei. Note only faint BAG-1 positivity in the deeper, basal cell layer of the epithelium; ×1000. *19*, human prostate, showing strong cytoplasmic BAG-1 immunostaining in basal cells along the basement membrane but little or no staining of the overlying differentiated secretory cells facing the lumen of the gland; ×400. *20* and *21*, testes from human and mouse, respectively, showing examples of strong perinuclear and cytosolic BAG-1 immunostaining of spermatogonia (methylgreen counterstain; ×400) and BAG-1 immunopositivity of spermatozoa (×200), respectively. Note that the testes from aged human is atrophic compared with young mouse. *22*, proliferative human mammary gland alveoli with BAG-1 immunostaining within both cytoplasm and nuclei of mammary epithelial cells; ×400. *23*, murine ovary with BAG-1 immunopositive nuclei in luteal cells but not in the granulosa cells of a secondary follicle; ×400. *24*, human thymus, demonstrating strong BAG-1 immunopositivity in reticuloepithelial cells but no apparent immunostaining of thymocytes; ×200. *25*, human splenic white pulp demonstrating only weak BAG-1 immunopositivity of neutrophils and endothelium of splenic venous sinusoids (*arrows*) but absence of BAG-1 in lymphoid cells (methyl green counterstain); ×400. *26* and *27*, bone marrow from mouse and human, respectively, demonstrating strong BAG-1 immunostaining of megakaryocyte nuclei (×400) and moderate intensity immunostaining of mature monocytes (*arrow*) and granulocytes, with relatively less BAG-1 immunoreactivity in more immature hemopoeitic cells (×1000), respectively. *28* and *29*, human brain (frontal cortex) and mouse spinal cord, presenting examples of strong nuclear BAG-1 immunostaining in neurons. Note that surrounding macroglia (*arrows*) are immunonegative (methyl green counterstain; ×400). *30* and *31*, adrenal gland from mouse at low (×80) and high (×1000) magnification, illustrating predominantly cytosolic BAG-1 immunostaining of cortical cells and mostly nuclear immunostaining of medullary cells.

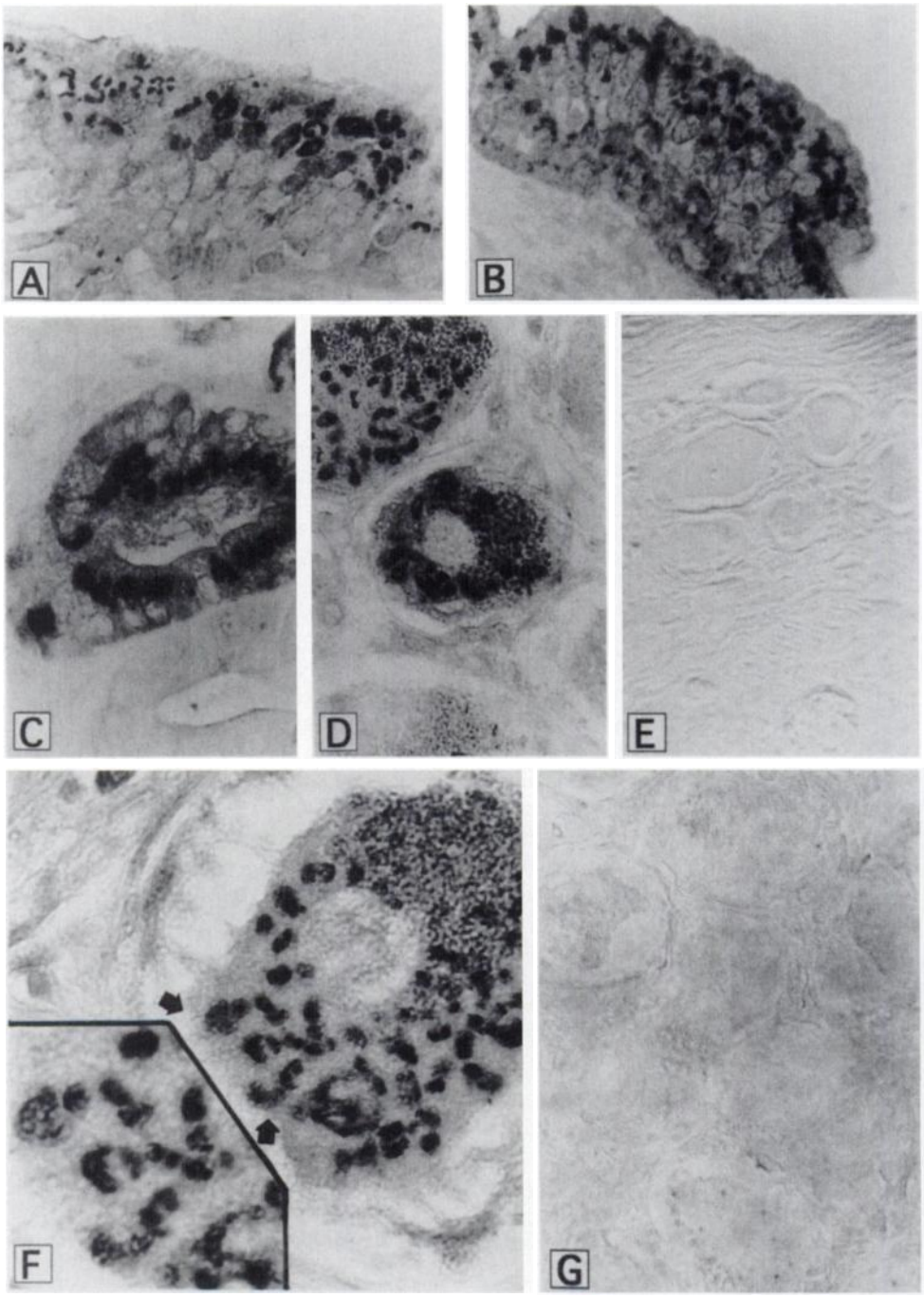

Fig. 9. Light- and laser-scanning microscopic analysis of BAG-1 protein demonstrates association with mitochondria. BAG-1 immunostained paraffin-embedded tissue sections (3 μm) were examined by light (*A–E*) or laser-scanning (*F* and *G*) microscopy. Typical examples of organellar immunostaining are presented from human pattern pseudocolumnar bronchial epithelium (*A*); transitional epithelium (*B*); gastric gland (*C*); and neurons of a dorsal root ganglion (*C*), as shown for sensory ganglia neurons on *D* (×1000). Laser scanning analysis of dorsal root ganglion neurons is presented in *F* (×3000). The *inset* shows a higher magnification view of immunostained mitochondria derived from the region indicated by the *arrows* (×5000). In *E* (×4000) and *G* (×3000), the anti-BAG-1 monoclonal antibody was preadsorbed with GST-BAG-1 fusion protein as a control for immunospecificity.

some striking similarities with BAG-1. Similar to BAG-1, the bFGF mRNA encodes a shorter ~18 kDa form of bFGF, which is predominantly found in the cytosol and which arises from a traditional AUG codon, as well as longer ~22–24-kDa bFGF isoforms that reside in the nucleus and arise from upstream, in-frame, noncanonical CUG codons (30). It may also be relevant that the nuclear targeting NH_2-terminal sequences of these longer isoforms of bFGF constitute a proline-rich domain similar to the predicted the NH_2-termini of the human and mouse BAG-1L proteins (31).

Despite the presence of a potential NLS and some similarity to the nuclear targeting NH_2-terminus of high molecular weight bFGF, the BAG-1L protein was also found to some extent in the nonnuclear fraction by subcellular fractionation, suggesting that its import into the nucleus is regulated rather than constitutive. In this regard, the immunohistochemical analysis of normal tissues implied dynamic regulation of BAG-1 entry into or exit from the nucleus in some types of cells. For example, whereas the basal cell layer of keratinocytes contained both nuclear and cytosolic BAG-1 immunostaining, the more differentiated cells in the upper layers of the epidermis generally contained only cytosolic BAG-1. In addition, specimen to specimen variation in the location of BAG-1 in the prostate gland also implied regulation of nuclear import or export. We have also observed variations among breast cancer specimens with regard to whether they contain BAG-1 in both cytosol and nucleus *versus* in the cytosol only.[7] Although the shorter mouse originally described human and mouse BAG-1 proteins lack regions with clear similarity to NLS

[7] M. Krajewska, C. Reynolds, S. Krajewski, S. Takayama, C. V. Clevenger, and J. C. Reed. Loss of nuclear BAG-1 immunostaining associated with reduced estrogen and progesterone receptor expression in breast cancer, submitted for publication.

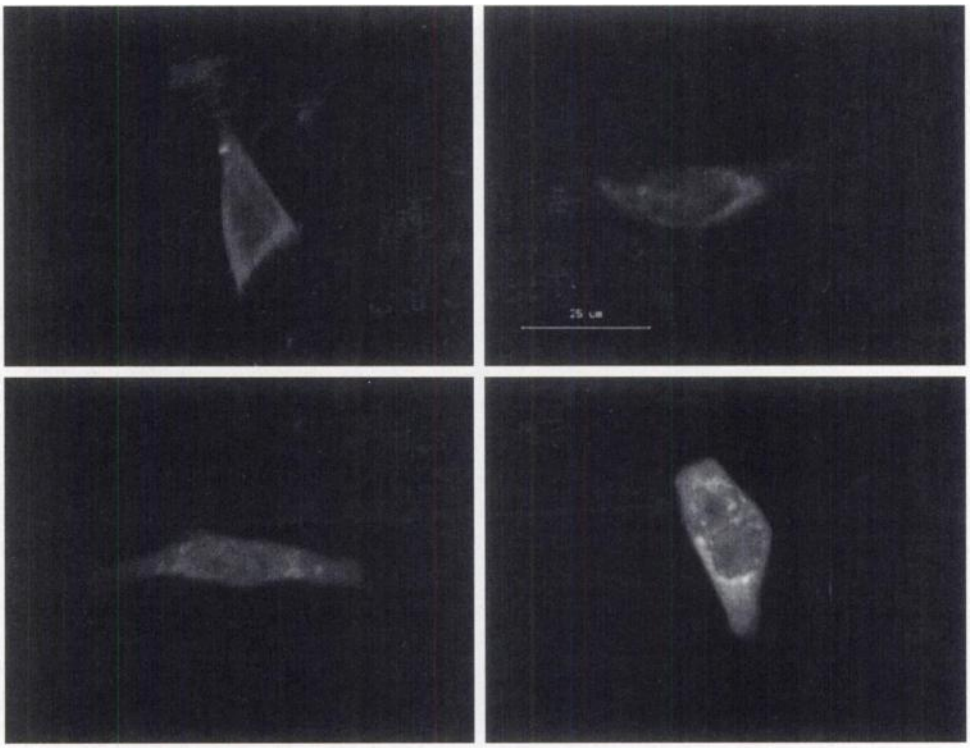

Fig. 10. Bcl-2 alters intracellular distribution of GFP-BAG-1. HeLa cells were transiently transfected with a plasmid encoding GFP-BAG together with equal amounts of either pRc/CMV control (*upper left panel*) or pRc/CMV-Bcl-2 (*other panels*) plasmids. Two days later, images were taken of representative cells using a confocal microscope.

motifs, the mouse BAG-1 protein has been shown to interact with retinoic acid receptors.[8] Thus, it is possible that the shorter BAG-1 protein could also gain entry into the nucleus through its interactions with other proteins. Moreover, because the BAG-1M protein (also known as RAP46) has been reported to interact with other steroid hormone receptors, including as ER, glucocorticoid receptor, progesterone receptor, and androgen receptor, its location theoretically could be controlled in part by associations with these receptors as they traffic between cytosol and nucleus in response to steroid hormones.

In many types of cells, BAG-1 immunostaining was present in the cytosol or in association with cytosolic organelles that morphologically resembled mitochondria, rather than in the nucleus. Association of BAG-1 with mitochondria is consistent with the reported interaction of this protein with Bcl-2 (1). The Bcl-2 protein resides in the outer mitochondrial membrane, oriented toward the cytosol. The immunostaining of BAG-1 seen around the circumference of mitochondria at high magnification by light and laser scanning microscopy supports the idea of BAG-1 association with the outer membrane of mitochondria and is highly reminiscent of previous results obtained for Bcl-2 by the same methods (21). Further studies including immuno-electron microscopy, however, are required for definitive confirmation of BAG-1 association with the outer membrane. BAG-1 immunostaining also occurred in a perinuclear distribution in some types of cells, not unlike Bcl-2 and some of its homologues that have been shown to reside in the nuclear envelope and parts of the endoplasmic reticulum (ER), as well as outer mitochondrial membranes (21, 32). Moreover, when coexpressed in cells, Bcl-2 resulted in targeting of a GFP-BAG-1 fusion protein to perinuclear membranes and cytosolic structures that probably represent mitochondria, providing direct evidence that Bcl-2 can alter the intracellular distribution of the BAG-1 protein. It should be noted, however, that an organellar or perinuclear pattern of BAG-1 immunostaining was not seen in all cell-types that are known to express Bcl-2 *in vivo*. Thus, unidentified events presumably determine whether BAG-1 is recruited to the organellar or nuclear membranes where Bcl-2 resides. Although many possibilities exist, one such event could be dimerization of Bcl-2 with antagonists such as Bax or BAD, which conceivably might prevent Bcl-2 from binding to BAG-1.

It remains to be determined whether the BAG-1L and BAG-1M proteins can interact with the same proteins reported for BAG-1. Previous studies have shown that the NH_2-terminal first 89 amino acids of the mouse BAG-1 protein are expendable for binding to Hsc70, Hsp70, Bcl-2, Raf-1, HGF-R, and PDGF-R (1, 5, 7, 11).[5] Thus, the NH_2-terminal Glu-Glu repeat domain and ubiquitin-like domains of BAG-1 are not required for those protein interactions. In contrast, the COOH-terminal 47 amino acids of mouse BAG-1 are critical for binding to Hsc70, Hsp70, and Raf-1, and the last 84 amino acids of BAG-1 are sufficient for binding to HGF-R and PDGF-R. Because BAG-1L differs from BAG-1 at the NH_2 rather than COOH terminus, it seems likely that it should also bind to these same proteins. Moreover, as shown here, BAG-1, BAG-1M, and BAG-1L all retain the ability to interact with Hsc70. Thus, BAG-1 and its variants BAG-1L and BAG-1M may have the potential to target Hsp70/Hsc70 family proteins to different compartments within cells, presumably facilitating the interactions of Hsp70/Hsc70 family proteins with other proteins in the cytosol, at the mitochondrial surface, or in the nucleus.

The survey of 67 human tumor lines performed here indicates that BAG-1 protein levels can vary widely among malignant cells. However, compared with other tumor lines, BAG-1 protein levels were consistently at high levels in leukemia and lymphoma cell lines, which contained high levels of BAG-1 protein in seven of seven cases. We cannot determine whether the relatively high levels of BAG-1 seen in leukemias and lymphomas as well as many types of solid tumor cell lines represent a pathological increase in the expression of this anti-apoptotic protein in the absence of direct comparisons with purified populations of the appropriate normal cell counterparts. However,

[8] R. Liu, S. Takayama, Y. Zheng, B. Froesch, G-Q. C., X. Zhang, J. C. Reed, and X-K. Zhang. Interaction of BAG-1 with retinoic acid receptor and its inhibition of retinoic acid-induced apoptosis in cancer cells, J. Biol. Chem., in press.

Table 2 *Summary of BAG-1 immunoblot data for human tumor cell lines*

Data represent estimated BAG-1 protein levels (ng per 50 μg of total protein) based on quantification of immunoblot data by densitometric scanning and extrapolation from a GST-BAG-1 standard curve. Data were scored as: 0, undetectable; +/−, 1 to ≤5 ng/50 μg; +, 5 to ≤10 ng/50 μg; ++, 10 to ≤15/50 μg; +++, 15 to ≤20/50 μg; and ++++, >20 ng/50 μg). Tumor lines are grouped by categories.

	BAG-1	BAG-1_M	BAG-1_L
Breast			
BT-549	+++	0	+
HS578T	+	0	0
MCF-7	++++	+/−	+/−
MCF7ADR/RES	+	+/−	+/−
MDA-MB-231	++++	+/−	+
MDA-MB-435	+++	+/−	+
MDA-N	+++	+/−	+/−
T47D	+	0	0
Colon			
COLO205	+	0	0
HCT-15	+++	+/−	+/−
HCT-116	+++	0	0
HCC-2998	+++	0	0
HT29	+/−	0	0
KM-12	++++	+/−	+/−
SW-620	++++	+/−	+/−
CNS			
SF-268	+++	+/−	+/−
SF-295	+++	0	0
SF-539	0	0	0
SNB-19	0	0	0
SNB-75	++	0	+/−
U251	+++	+/−	+/−
Leukemia/Lymphoma			
CCRF-CEM	+	−	+/−
HL-60	+++	+/−	0
K562	++++	+/−	+/−
MOLT-4	+++	+/−	+/−
RPMI-8226	+++	+/−	0
RS11846	++++	+	+
Jurkat	+++	+/−	++
SR	+++	0	0
Lung			
A549	++	0	+
EKVX	++++	+	++
HOP-62	+++	0	0
HOP-92	+/−	+/−	0
NCI-H322M	0	0	0
NCI-H226	+/−	+/−	+/−
NCI-H23	+/−	+/−	+/−
NCI-H522	+/−	0	0
NCI-H460	0	0	0
Melanoma			
LOX-IMVI	+/−	0	0
MALME-3M	++++	+/−	+/−
M14	++	0	0
SK-MEL-2	0	0	+/−
SK-MEL-5	++	+/−	+/−
SK-MEL-28	+	0	0
UACC-62	+	0	+/−
UACC-257	+	0	0
Ovarian			
IGROV1	++	0	+
OVCAR-3	++++	+/−	+
OVCAR-4	+/−	0	+/−
OVCAR-5	+/−	0	0
OVCAR-8	+/−	+/−	+/−
SK-OV-3	+	−	++
Prostate			
LNCap	++	+/−	++
DU-145	+++	+	++
PC-3	++	+/−	+/−
PPC-1	+++	+/−	+
ALVA-31	++	+/−	+/−
Tsu-PRL	+	0	+/−
JCA-1	+/−	0	+/−
Renal			
786-0	+++	+/−	+/−
A498	+	0	0
ACHN	+++	0	0
CAKI-1	0	0	0
RXF-393	+/−	0	0
SN12C	+++	+/−	+
TK-10	+++	0	0
UO-31	+	0	0

immunohistochemical analyses of some of the corresponding normal tissues, such as hemopoietic and lymphoid organs, suggest this might be the case.

With few exceptions, the ~36-kDa BAG-1 protein was clearly the most abundant form of BAG-1 found in tumor lines. The BAG-1M (RAP46) protein reproducibly constituted <10% of the total BAG-1 in these malignant cell lines and was the least abundant isoform of BAG-1. In contrast, the BAG-1L protein was more variable in its expression, and in a few instances BAG-1L levels approached or were equivalent to the levels of ~36-kDa BAG-1 in tumor lines such as the breast cancer BT-549, the prostate cancer lines DU-145 and LN-CaP, and the leukemia line Jurkat. Indeed, breast cancer, prostate cancer, and leukemia cell lines were the most consistent expressors of the BAG-1L protein, with seven of seven prostate, seven of eight breast, and four of five leukemia cell lines containing immunodetectable levels of this protein. An intriguing possibility is that BAG-1L, with its proclivity for nuclear targeting, may contribute to the regulation of nuclear hormone receptor function in these types of tumors, given the prominent role played by androgen receptor, ER, and glucocorticoid receptor in cancers of the prostate, breast, and lymphoid organs, respectively. Also of potential relevance to the issue of BAG-1 and steroid hormone receptors was the finding that ovary and testis contained the highest relative amounts of BAG-1L protein among normal tissues, given that these tissues represent the principal sources of estrogen and androgen production. Thus, unidentified tissue-specific factors presumably influence the extent to which translation initiation can occur at the upstream noncanonical CTG codons relative to the usual ATG codon start-site within BAG-1 mRNAs. It remains to be determined whether dynamic fluctuations in the relative ratios of BAG-1 and BAG-1L play a role in the apparent variations in the intracellular location of BAG-1 immunostaining in steroid hormone-dependent tissues such as the prostate gland.

In summary, the findings presented here demonstrate the existence of additional forms of the BAG-1 protein in both humans and mice, including one that appears to arise through translation initiation from an upstream CTG within BAG-1 transcripts. The expression of BAG-1 is highly tissue specific and can vary in some instances with differentiation in particular cell lineages. The intracellular locations of BAG-1 proteins also differ among cell types, suggesting that interactions with other proteins modulate the locations of BAG-1 within cells. Delineating the mechanisms that control the translation initiation decision that gives rise to BAG-1L, BAG-1M, or BAG-1; contrasting the functions and intracellular locations of the BAG-1, BAG-1M, and BAG-1L proteins; and understanding how BAG-1 expression and function may become altered in cancer represent goals for the future.

ACKNOWLEDGMENTS

We thank T. Brown for manuscript preparation and Xiaokun Xiao for technical assistance.

REFERENCES

1. Takayama, S., Sato, T., Krajewski, S., Kochel, K., Irie, S., Millan, J. A., and Reed, J. C. Cloning and functional analysis of BAG-1: a novel Bcl-2 binding protein with anti-cell death activity. Cell, *80:* 279–284, 1995.
2. Clevenger, C. V., Thickman, K., Ngo, W., Chang, W-P., Takayama, S., and Reed, J. C. Role of Bag-1 in the survival and proliferation of the cytokine-dependent lymphocyte lines, Ba/F3 and Nb2. Mol. Endocrinol., *11:* 608–618, 1997.
3. Schulz, J. B., Bremen, D., Reed, J. C., Lommatzsch, J., Takayama, S., Wullner, U., Loschmann, P-A., Klockgether, T., and Weller, M. Cooperative interception of neuronal apoptosis by BCL-2 and BAG-1 expression: prevention of the cytokine activation and reduced production of reactive oxygen species. J. Neurochem., *69:* 2075–2086, 1997.
4. Terada, S., Fukuoka, K., Fujita, T., Komatsu, T., Takayama, S., Reed, J. C., and Suzuki, E. Anti-apoptotic proteins, bag-1 and bcl-2, improve survival and antibody

production by hybridoma cells under conditions of thymidine excess and serum deprivation. Cytotechnology, *25:* 17–23, 1997.
5. Takayama, S., Bimston, D. N., Matsuzawa, S., Freeman, B. C., Aime-Sempe, C., Xie, Z., Morimoto, R. J., and Reed, J. C. BAG-1 modulates the chaperone activity of Hsp70/Hsc70. EMBO J., *16:* 4887–4896, 1997.
6. Danen-van Oorschot, A. A. A. M., den Hollander, A., Takayama, S., Reed, J. C., van der Eb, A. J., and Noteborn, M. H. M. BAG-1 inhibits p53-induced but not apoptin-induced apoptosis. Apoptosis, *2:* 395–402, 1997.
7. Bardelli, A., Longati, P., Albero, D., Goruppi, S., Schneider, C., Ponzetto, C., and Comoglio, P. M. HGF receptor associates with the anti-apoptotic protein BAG-1 and prevents cell death. EMBO J., *15:* 6205–6212, 1996.
8. Jeffers, M., Rong, S., and Woude, G. F. Hepatocyte growth factor/scatter factor-Met signaling in tumorigenicity and invasion/metastasis. J. Mol. Med., *74:* 505–513, 1996.
9. Frisch, S. M., and Francis, H. Disruption of epithelial cell-matrix interactions induces apoptosis. J. Cell Biol., *124:* 619–626, 1994.
10. Adachi, M., Sekiya, M., Torigoe, T., Takayama, S., Reed, J. C., Miyazaki, T., Minami, Y., Taniguchi, T., and Imai, K. Interleukin-2 (IL-2) upregulates *BAG-1* gene expression through serine-rich region within IL-2 receptor beta c chain. Blood, *88:* 4118–4123, 1996.
11. Wang, H-G., Takayama, S., Rapp, U. R., and Reed, J. C. Bcl-2 interacting protein, BAG-1, binds to and activates the kinase Raf-1. Proc. Natl. Acad. Sci. USA, *93:* 7063–7068, 1996.
12. Hohfeld, J., and Jentsch, S. GrpE-like regulation of the hsc70 chaperone by the anti-apoptotic protein bag-1. EMBO J., *16:* 6209–6216, 1997.
13. Takayama, S., Kochel, K., Irie, S., Inazawa, J., Abe, T., Sato, T., Druck, T., Huebner, K., and Reed, J. C. Cloning of cDNAs encoding the human BAG1 protein and localization of the human *BAG1* gene to chromosome 9p12. Genomics, *35:* 494–498, 1996.
14. Packham, G., Brimmell, M., and Cleveland, J. L. Mammalian cells express two differently localized Bag-1 isoforms generated by alternative translation initiation. Biochem. J., *328:* 807–813, 1997.
15. Zeiner, M., and Gehring, U. A protein that interacts with members of the nuclear hormone receptor family: identification and cDNA cloning. Proc. Natl. Acad. Sci. USA, *92:* 11465–11469, 1995.
16. Reed, J., Meister, L., Cuddy, M., Geyer, C., and Pleasure, D. Differential expression of the *bcl-2* proto-oncogene in neuroblastomas and other human neural tumors. Cancer Res., *51:* 6529–6538, 1991.
17. Krajewski, S., Zapata, J. M., and Reed, J. C. Detection of multiple antigens on Western blots. Anal. Biochem., *236:* 221–228, 1996.
18. Krajewski, S., Krajewska, M., Shabaik, A., Miyashita, T., Wang, H-G., and Reed, J. C. Immunohistochemical determination of *in vivo* distribution of bax, a dominant inhibitor of bcl-2. Am. J. Pathol., *145:* 1323–1333, 1994.
19. Krajewski, S., Krajewska, M., Shabaik, A., Wang, H-G., Irie, S., Fong, L., and Reed, J. C. Immunohistochemical analysis of *in vivo* patterns of Bcl-X expression. Cancer Res., *54:* 5501–5507, 1994.
20. Krajewski, S., Bodrug, S., Krajewska, M., Shabaik, A., Gascoyne, R., Berean, K., and Reed, J. C. Immunohistochemical analysis of Mcl-1 protein in human tissues: differential regulation of Mcl-1 and Bcl-2 protein production suggests a unique role for Mcl-1 in control of programmed cell death *in vivo*. Am. J. Pathol., *146:* 1309–1319, 1995.
21. Krajewski, S., Tanaka, S., Takayama, S., Schibler, M. J., Fenton, W., and Reed, J. C. Investigation of the subcellular distribution of the bcl-2 oncoprotein: residence in the nuclear envelope, endoplasmic reticulum, and outer mitochondrial membranes. Cancer Res., *53:* 4701–4714, 1993.
22. Chomczynski, P. One-hour downward alkaline capillary transfer for blotting of DNA and RNA. Anal. Biochem., *201:* 134–139, 1992.
23. Sambrook, J., Fritsch, E. F., and Maniatis, T. Molecular Cloning: A Laboratory Manual, Ed. 2. Cold Spring Harbor, NY: Cold Spring Harbor Laboratory, 1989.
24. Hennighausen, L., and Lubon, H. Interaction of protein with DNA *in vitro*. Methods Enzymol., *152:* 721–735, 1987.
25. Kozak, M. Recognition of AUG and alternative initiator codons is augmented by G in position +4 but is not generally affected by the nucleotides in positions +5 and +6. EMBO J., *16:* 2482–2492, 1997.
26. Grunert, S., and Jackson, R. J. The immediate downstream codon strongly influences the efficiency of utilization of eukaryotic translation initiation codons. EMBO J., *13:* 3618–3630, 1994.
27. Robbins, J., Dilworth, S. M., Laskey, R. A., and Dingwall, C. Two interdependent basic domains in nucleoplasmin nuclear targeting sequence: identification of a class of bipartite nuclear targeting sequence. Cell, *64:* 615–623, 1991.
28. Dingwall, C., and Laskey, R. A. Nuclear targeting sequences—a consensus? Trends Biochem. Sci., *16:* 478–481, 1991.
29. Harrison, C. J., Hayer-Hartl, M., Di Liberto, M., Hartl, F-U., and Kuriyan, J. Crystal structure of the nucleotide exchange factor grpE bound to the ATPase domain of the molecular chaperone DnaK. Science (Washington DC), *276:* 431–435, 1997.
30. Florkiewicz, R. Z., Baird, A., and Gonzalez, A. M. Multiple forms of bFGF: differential nuclear and cell surface localization. Growth Factors, *4:* 265–275, 1991.
31. Quarto, N., Finger, F. P., and Rifkin, D. B. The NH2-terminal extension of high molecular weight bFGF is a nuclear targeting signal. J. Cell. Physiol., *147:* 311–318, 1991.
32. Monaghan, P., Robertson, D., Andrew, T., Amos, S., Dyer, M. J. S., Mason, D. Y., and Greaves, M. F. Ultrastructural localization of bcl-2 protein. J. Histochem. Cytochem., *40:* 1819–1825, 1992.

Expression and Location of Hsp70/Hsc-Binding Anti-Apoptotic Protein BAG-1 and Its Variants in Normal Tissues and Tumor Cell Lines

Shinichi Takayama, Stanislaw Krajewski, Maryla Krajewska, et al.

Cancer Res 1998;58:3116-3131.